**Charles University in Prague**

Faculty of Science

Department of Physical and Macromolecular Chemistry

# Light Scattering and Fluorescence Studies of Poly(ethylene oxide)-*block*-poly(ε-caprolactone) Self-assembled Nanoparticles

Radek Šachl

DIPLOMA THESIS

Praha 2007

This diploma thesis was worked out at the Department of Physical and Macromolecular Chemistry at the Faculty of Science of the Charles University. My supervisor was RNDr. Miroslav Štěpánek, Ph.D. and the consultant Doc. Dr. Martin Hof, DSc. All light scattering measurements were carried out at the Department of Physical and Macromolecular Chemistry while most of the fluorescence experiments were done at the J. Heyrovský Institute of Physical Chemistry of the Academy of Sciences of the Czech Republic in the team of Doc. Hof. All AFM images were obtained at the Institute of Macromolecular Chemistry of the Academy of Sciences of the Czech Republic in collaboration with Ing. Milena Špírková, CSc.

I declare that I have elaborated the thesis on my own. If other already published results are used, they are included in the list of references. I agree with lending the thesis to anyone who may be interested.

Praha, 12.2.2007

## Acknowledgements

The list of abbreviations and used symbols enclosed to this thesis is essentially shorter than would be a list of persons who I would like to acknowledge at this place. Even if the list appeared to me at last to be complete, it would not be in reality as is probably not the list of abbreviations. Therefore, before acknowledging some people by name, I would like to thank everybody who has anyhow contributed to this work at first. I especially express my thanks to my supervisor RNDr. Mirek Štěpánek, Ph.D. for many fruitful hints and all the help he offered me during the work on my thesis. Many thanks belong also to Doc. Dr. Martin Hof, DSc. for a nice collaboration with him, for having accepted me as one of his students and especially for his friendly attitude. I am thankful to Ing. Milena Špírková, CSc. for the worth help with AFM measurements as well. With all my heart, I thank to my parents, grandparents, my brother and especially to the closest person to me, Šárka Lukschová, for all that what cannot be expressed by words.

## Content

## 1.1. First Introduction

My favourite writer Erich Kästner liked introductions so much that he used to write in his books the first and second introduction, *i.e.*, the introduction to introduction and the introduction itself. Therefore, I recommend all the readers who like introductions to draw their attention to my first reference[A] and those readers who do not like them to proceed directly to the section Motivations and Our Goals. All other readers can then continue with the following Second Introduction.

## 1.2. Second Introduction

It is really almost useless to mention at this particular place any general information on the self-assembling behaviour of polymers, since these facts can be found in many other publications, including proceeding diploma thesis elaborated by my colleagues from the group of prof. Procházka. To this date, almost 70 000 publications devoted to problems of self-assemblies have appeared in the scientific literature. This huge number only demonstrates how promising might be this topic. That should not surprise us after realizing that a living cell can be regarded as a highly organized self-assembled system of proteins, lipids and polysaccharides. To gain insight into such a complicated system, one has firstly to understand simpler structures, to which micelles or vesicles belong without any doubt. The investigation of micelles or vesicles is in addition motivated by their broad applications in development of drug delivery devices, in emulsions or detergents.

The micelles are also the main point of interest of the whole team of prof. RNDr. Karel Procházka, DrSc., in which I elaborated my diploma thesis. Most of the work has been done on the self-assembly of polystyrene-*block*-poly(methacrylic acid), on polystyrene-*block*-poly(ethylene oxide) and newly on polystyrene-*block*-poly(2-vinylpyridine)-*block*-poly(ethylene oxide) by means of light-scattering, various fluorescence techniques, atomic force microscopy and electrophoresis. Recently, we started to investigate biocompatible polymers and to solve problems of DNA condensation.

[A] Erich Kästner, *Drei Männer im Schnee*; Deutscher Taschenbuch Verlag GmbH & Co. KG: München, 2002.

## 2. Motivations and Our Goals

In the published papers on PCL-PEO nanoparticles, most of the attention has been paid to the biodegradation of the PCL hydrophobic domain,[1,2] to the loading efficiency for fluorescent probes[3,4] and to the release kinetics of loaded compounds.[3,4,5,6] However, almost no studies appeared that were interested in proper characterization of self-assembled PCL-PEO particles, except studies published by Vangeyte *et al.*[7,8] Nevertheless, these studies deal with PCL-PEO with a short PCL block only. That is why we decided to characterise nanoparticles formed from PCL-PEO block copolymers with the length of the PCL chain comparable with the length of the PEO chain or even longer.[9]

Our efforts mainly concentrated on:

- Finding the optimal organic solvent or a mixture of the solvent and water for all PCL-PEO polymers we used, from which the polymers could be successfully transferred into water.
- Preparing defined nanoparticles with satisfying polydispersity and characterising them afterwards by means of SLS, QELS and AFM.
- Finding what type of particles exists in water, *i.e.*, whether micelles or vesicles were formed.
- Investigating how the properties of self-assembled particles can be tuned by changes in the preparation protocol, *i.e.*, by changes in concentration and used organic solvent/water ratio.
- Finding whether the aggregation numbers and hydrodynamic radii of the nanoparticles satisfy theoretical scaling relations.
- Exploring how the organic solvent used to dissolve the polymers influences the populations of fluorescent probes PRODAN and LAURDAN inside and outside the hydrophobic PCL domain. To do that, we applied steady-state and time-resolved fluorescence spectroscopy and fluorescence solvent relaxation technique.
- Following, if possible, changes in hydration of the PCL domain, caused by its swelling due to addition of the organic solvent into water containing nanoparticles.

## 3. Poly(ε-caprolactone)-*block*-poly(ethylene oxide) in Literature

Poly(ε-caprolactone)-*block*-poly(ethylene oxide), PCL-*b*-PEO, belongs to the class of neutral amphiphilic block copolymers[7,8,10,11] and consists of a hydrophobic PCL part and a hydrophilic PEO part. Such a polymer has, of course, a pronounced tendency to self-assemble in water into structures with a hydrophobic and hydrophilic domain. Since the PCL block is biodegradable in a living organism[1,2] and the PEO block is known to be biocompatible due to low adsorption affinity to proteins, PCL-PEO can be used in medicine as a carrier of drugs purely soluble in water.[3,5,6] For this purpose, only a few polymers come into account because the selection of core-forming blocks is limited to few polymers such as poly(propylene oxide),[12,13] PPO, poly(β-benzyl L-aspartate),[14] PBLA, poly(D,L-lactide),[15] PDLLA, or poly(γ-benzyl-L-glutamate),[16] PBLG.

### 3.1.1. Synthesis of PCL-PEO and Preparation of Nanoparticles

One of possible ways to synthesize PCL-PEO is the sequential anionic polymerization of ethylene oxide, EO, followed by ring-opening polymerization of ε-caprolactone, CL.[17] The anionic polymerization of EO is usually initiated by triethylenglycol monomethyl ether added with KOH, which serves as a catalyst at 115 °C. After the reaction reaches its equilibrium state, the hydroxyl-terminated PEO is purified and activated with trialkylaluminium for the next polymerization with CL, which is carried out at 25 °C in methylene chloride. The final product is obtained after precipitation in heptane and following dialysis from 80% THF/water solution against pure water. By this procedure, one can obtain PCL-PEO polymers with different length of both PCL and PEO chains.

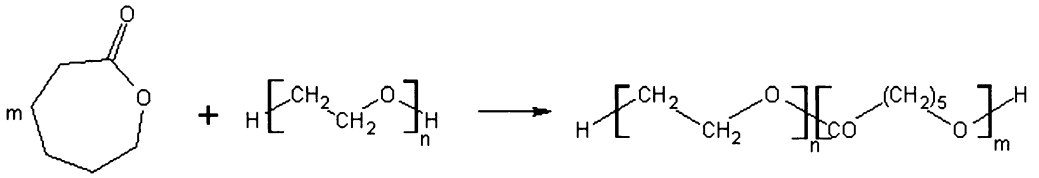

Having the synthesised PCL-PEO, the next essential step is to dissolve the polymer in water and to induce the self-assembling process. However, the direct dissolution of the polymer in water needs not to be always possible. Vangeyte *et al.*[8] succeeded in dissolving the $PCL_m$-$PEO_{114}$ directly in water at room temperature only when the PCL block contained maximally three monomer units. In order to dissolve PCL-PEO with more than three

monomer units in water, Vangeyte *et al.* tried to increase the temperature to 82 °C, which helped for PCL-PEO containing 19 PCL units. As revealed by the small angle X-ray scattering measurements, the PCL-PEO particles prepared by this method were spherical micelles of about 20 nm in diameter. Neither the further increase of temperature nor the prolongation of heating the polymer-water solution was sufficient for dissolving polymers with the longer PCL chain.

The next frequently used approach to transfer the polymer into water is based on dissolving the polymer in an organic solvent and dialysing the polymer solution against water or step-by-step against solutions with decreasing content of the initial organic solvent. Unfortunately, in the case of the PCL-PEO, this method leads to large unstable aggregates with units of micrometers in size.[7]

The formation of large aggregates can be prevented successfully if the polymer organic solution is added drop-by-drop into an excess of water or if water is added slowly to the polymer solution and dialysed afterwards. In general, the formed nanoparticles are considerably larger (30-80 nm in diameter) than by using the direct dissolution of the PCL-PEO polymer in water. However, one has to bear in mind that, in this particular case, the molar masses and the sizes of formed nanoparticles depend on the preparation protocol, *i.e.*, on the organic solvent used, on whether the polymer solution was added into water or *vice versa* or on the concentration of the polymer in the solution.[7]

### 3.1.2. Biodegradation of PCL

Polyesters such as poly(ε-caprolactone), polylactide or poly(glycolic acid) undergo hydrolysis inside a body by interacting with body fluids, enzymes, *e.g.* Lipase Pseudomonas, Lipase PS, and cells. During the hydrolysis, molecules with shorter chains, *i.e.*, with about six monomer units, are produced. After having been degraded, these molecules are removed from a living organism easily.[1]

*In vitro*, the kinetics of biodegradation of PCL nanoparticles by Lipase PS can be followed by static light scattering. Since the PCL particles are insoluble in water, the classical Michaelis-Menten model, usually applied for homogenous systems, does not suit to describe the kinetics of PCL degradation. Nowadays, it is considered that the enzymatic degradation involves two essential steps: (1) the adsorption of Lipase PS onto the nanoparticles and (2) the degradation of the PCL from the surface inside the nanoparticles. Light scattering data show that the initial degradation rate increases with the increasing

concentration of Lipase PS and that the enzyme loses its activity gradually. On the other hand, the rate of degradation of the whole particle does not depend on the concentration of the particles in the solution, which suggests that the PCL particles are 'consumed' one-by-one.[1,2]

### 3.1.3. Incorporation and Release of Hydrophobic Probes from PCL-PEO

As mentioned above, nanoparticles formed from the PCL-PEO polymer can be used in developing drug-delivery devices.[18] To do this, one has to understand properly which parameters influence the incorporation of hydrophobic probes (drugs) into the PCL-PEO particles because not every probe that one wishes to deliver inside a body is incorporated into the particles efficiently. Soo *et al.*[3] demonstrated this different behaviour of various probes on the PCL-PEO nanoparticles using two fluorescent probes, namely benzo[a]pyrene and cell-tracker CM-DiI, DiI. While the maximum loading efficiency for DiI reached 87%, in the case of benzo[a]pyrene it was only 32%. These loading efficiencies correspond to the partition coefficients 5800 for DiI and 700 for benzo[a]pyrene.

Similarly to the difference in partition coefficients, the rate with which the drugs are released from the hydrophobic domain of the particles depends on the type of the probe and also the polymer as shown for the release of cyclosporine A from PCL-PEO particles or Cremophor EL micelles, respectively.[4,6] Cyclosporine A is a drug, which suppresses immune response of the organism after transplantation. Because of a very pure solubility of this compound in water (23 μg/ml), it has been dissolved in an ethanolic solution of Cremophor EL, polyester of glycerol, so far. Unwanted properties of this delivery system, such as observation of hypersensitivity and nephrotoxic reactions after administration of the medicament caused partly by Cremophor EL, or very high unsatisfying release rate of CsA from Cremophor EL micelles (77% of the drug content in 12 h), lead Aliabadi *et al.* to the idea to replace Cremophor EL by the non-toxic PCL-PEO. This resulted in better release kinetics (only 5,8% of CsA was released from the polymeric micelles within 12 h) and better loading efficiency (1.3 mg/ml).

### 3.2.1. Spectral Properties of PRODAN and LAURDAN

6-PROpionyl-2-(DimethylAmino)Naphthalene, PRODAN, and 6-LAURoyl-2-(DimethylAmino)Naphthalene, LAURDAN, have been the subject of various studies in

biomembrane research.[19-23,24] Both possess the same chromophore, which means that they both have uniform spectroscopic properties, but, due to the presence of the acyl chains with distinct lengths, they exhibit differences in localization in biomebranes or other hydrophobic systems, where they reside preferentially due to their high hydrophobicity.[22,25]

PRODAN has been firstly synthesised by Weber and Farris,[26] who intended to develop a fluorophore with a high sensitivity to its microenvironment. Such a probe should, as they assumed, exhibit large change in its dipole moment after excitation, so that the surrounding water molecules have to react upon this abrupt change, and so revealing the properties of the microenvironment. That is why they attached dialkylamino group, an electron donor, on one side of the naphthalene ring and an acyl group, often electron acceptor, on the opposite side of the aromatic ring. They hoped that this designed compound would undergo charge transfer, CT, in the excited state, leading to a large change in the dipole moment.

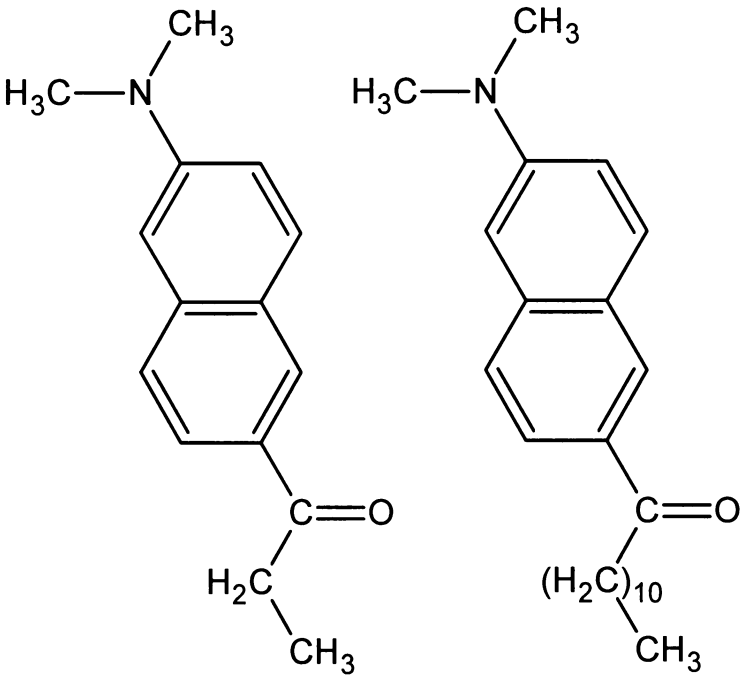


**Fig. 3.1.** Structure of PRODAN (on the left) and LAURDAN (on the right).

Although all results concerning proper estimation of the change of the dipole moment of PRODAN confirm that the change is really high, still, the obtained values are inconsistent with each other. Weber *et al.*[26] estimated the change at 20 D while Balter *et al.*[27] came to

only 8 D. Such a large change forces surrounding polar molecules to reorient in order to stabilize the excited state of the fluorophore, and the spectrum shifts to the red edge with time passing. The overall very large Stokes shifts are attributed to the charge transfer and to the specific solute-solvent interactions.[27] It is believed that the energy of the CT state is further lowered by the hydrogen bond between the partly charged carbonyl group and water molecule.

Indeed, the spectroscopic behaviour of PRODAN and LAURDAN is considered complex and involves, as shown on experiments with LAURDAN by Viard *et al.*,[28] an excited state reaction. LAURDAN can be excited into two different, but emitting states, *i.e.*, the locally excited state, LE, and the charge transfer, CT, state. The transition between these two states is observable in nonpolar media and could involve the rotation of the N-$(CH_3)_2$ group, which is necessary to extend charge separation on the nitrogen atom and to obtain the final CT state. The transition goes on so fast compared to the lifetime of the CT state that most of the detected fluorescence from polar medium comes from the unrelaxed or already relaxed CT state, and the fluorescence from the LE state need not to be taken into account in experiments with biomembranes, where the chromophore is located in polar environment.

### 3.2.2. Applications of PRODAN and LAURDAN / Solvent Relaxation

Solvent relaxation technique, SR, is very extensively used in biochemistry, especially in biomembrane research, but only rarely in clearing up properties of nonlipidic systems, *e.g.*, polymeric micelles or polymersomes, although it is applicable in this field, too.

In biomembrane research, SR allows us to monitor phase transition from the gel phase to the liquid-crystalline phase reliably because it is accompanied by the change of membrane's rigidity and increased water penetration into the phospholipid bilayer.[23,29,30] SR has been shown to be sensitive to the physical changes of biomembranes after inserting various membrane constituents, such as cholesterol or antibacterial peptides, into it as well.[30-32] Another factor that influences SR is the membrane curvature.[23,33] Though the Stokes shift, related to the degree of hydration, seems to be independent on the membrane curvature, the mobility of the microenvironment, described by the mean correlation time, $\tau_R$, (see section 4.2.5.3), increases when the bilayer is more bent. LAURDAN can be even used to follow the vesicle-to-micelle transition of phospholipid-amphiphile systems.[21]

What concerns nonlipidic polymeric micelles or vesicles, there are only a few studies present, some of them dealing with proper estimation of the critical micelle

concentration for low molecular surfactants,[34] with monitoring the hydration of tryptophan residues in peptides,[35] or with investigation of local environments in (star-like) surfactant macromolecules.[36,37,38] Our group has published a detailed study on hydration of poly(ethylene oxide) shells in polystyrene-*block*-poly(2-vinylpyridine)-*block*-poly(oxyethylene), PS-PVP-PEO, micelles recently.[25] The work shows that the relaxation of PATMAN in the PEO shell occurs on the nanosecond time-scale and that there are considerable pH-dependent changes in hydration of poly(ethylene oxide) units at the PVP/PEO interface.

# 4. Theoretical Part

### 4.1.1. Static Light Scattering[39,40]

Even though Rayleigh's scattered light is a disturbing element in methods such as fluorescence or Raman spectroscopy, it can provide very useful information on various polymer systems.

If the scattering particles of a diameter $d$ in a solution are small compared to the incident light ($d < \lambda/20$), the excess Rayleigh ratio, defined as

$$\Delta R(\theta, w) = \frac{I(\theta, w) - I(\theta, 0)}{I_0} r^2, \tag{1}$$

where $I_0$ is the intensity of the incident light, $I(\theta,w)$ is the intensity of the light scattered from the unit volume to the direction given by the angle between the incident and scattered light beams, $w$ the mass concentration of the scattering particles and $r$ is the distance between the scattering volume and the detector, does not depend on the angle of observation and from the dependence of $\Delta R$ on $w$, the weight averaged molar mass, $M_w$, and the second virial coefficient, $A_2$, can only be determined.

When the particle size exceeds $\lambda/20$, the interference of the scattered light from different domains of the particle starts being significant. As the consequence of this, the excess Rayleigh ratio changes with $\theta$, and this enables us to determine the z-averaged radius of gyration of the measured particles, $R_g$, as well.

The basic relationship used to obtain $M_w$, $R_g$ and $A_2$ for dilute solutions is the well-known equation

$$\frac{Kw}{\Delta R(\theta, w)} = \frac{1}{P(\theta) M_w} + 2A_2 w, \tag{2}$$

where $K = \dfrac{4\pi^2 n_0^2 (\mathrm{d}n/\mathrm{d}c)^2}{\lambda^4 N_A}$ is a constant containing the refractive index, $n_0$, of the solvent and refractive index increment of the polymer in the solvent, ($\mathrm{d}n/\mathrm{d}c$). Further, $P(\theta)$ is the particle scattering function, which describes the angular dependence of the intensity of the scattered light. When the particle is small with respect to the wavelength or the scattering angle is low, $P(\theta)$ can be expressed as[41]

$$P(\theta) = 1 - \frac{1}{3} R_g^2 q^2 \cong \frac{1}{1 + \frac{1}{3} R_g^2 q^2}. \tag{3}$$

In this expression $q$ stays for the size of the scattering vector $\boldsymbol{q}$ and equals

$$q = \frac{4\pi n_0}{\lambda} \sin(\theta/2). \tag{4}$$

By inserting eqn. (3) and eqn. (4) into eqn. (2), we finally obtain the following relation

$$\frac{Kc}{\Delta R(\theta, w)} = \frac{1}{M_w}\left(1 + \frac{16\pi^2 n_0^2}{3\lambda^2} R_g{}^2 \sin^2(\theta/2)\right) + 2A_2 w, \tag{5}$$

which is used in the so-called Zimm method, where $Kc/\Delta R$ is plotted against $kw+\sin^2(\theta/2)$. The extrapolation of the data to the zero angle and concentration provides us $M_w$, $R_g$ and $A_2$. Another approach is to plot $(Kc/\Delta R)^{1/2}$ against $(kw+\sin^2(\theta/2))^{1/2}$ according to Berry,

$$\sqrt{\frac{Kc}{\Delta R(\theta, w)}} = \sqrt{\frac{1}{M_w}\left(1 + \frac{8\pi^2 n_0^2}{3\lambda^2} R_g{}^2 \sin^2(\theta/2)\right)^2 + 2A_2 w}, \tag{6}$$

and to extrapolate the data in the same way as in the case of the Zimm method.

During the fitting one has to bare in mind the following aspects:

1. Eqn. (5) and (6) were derived from the approximation used in eqn. (3), whose precision decreases with the increasing angle of observation.
2. Impurities in the system such as dust or a minority of precipitated aggregates, which are both difficult to avoid completely, have a considerable influence on the intensity of the scattered light at low angles.
3. The higher order of the polynomial fit we use, the poorer is the robustness of the fit.

The next essential step of the extrapolation procedure is to choose the fitting method correctly. If the sample of interest contains particles with the radius not higher than 50 nm, the accuracy of obtained results does not depend on the method used. However, in the case of larger particles, the Zimm method ceases being reliable unlike the Berry method.[41]

### 4.1.2. Dynamic Light Scattering[39,40]

Particles that move irregularly in the solution enter and leave the space illuminated by the laser beam causing fluctuations in the intensity of scattered light, $I(t)$. These fluctuations can be measured and expressed by means of the normalized intensity autocorrelation function, $g_2(t)$,

$$g_2(t) = \frac{\lim_{T\to\infty} \frac{1}{T} \int_0^T I(t')I(t'+t)\mathrm{d}t'}{\langle I \rangle^2}. \tag{7}$$

This function has a close connection to the normalized autocorrelation function of the electric field, $\boldsymbol{E}(t)$, $g_1(t) = \frac{\lim_{T\to\infty} \frac{1}{T} \int_0^T \boldsymbol{E}(t')\boldsymbol{E}^*(t'+t)\mathrm{d}t'}{\langle \boldsymbol{E}\boldsymbol{E}^* \rangle}$,

$$g_2(t) = 1 + \beta |g_1(t)|^2, \tag{8}$$

where $\beta$ is the coherence factor accounting for deviation from the ideal correlation. By the polynomial fitting of the function $g_1(\tau)$ according to

$$\ln g_1(t) = \ln A - \Gamma t + \frac{\mu_2}{2} t^2, \tag{9}$$

where $A$ is the amplitude, $\Gamma$ the relaxation rate and $\mu_2$ the cumulant of the second order, the apparent diffusion coefficient, $D_{\mathrm{app}}$, can be determined reminding that

$$D_{\mathrm{app}}(q,w) = \frac{\Gamma}{q^2}. \tag{10}$$

Since the apparent diffusion coefficient depends on the concentration of particles in the solution and the angle of observation, it is extrapolated to the zero concentration and the zero angle of observation in the so called dynamic Zimm plot, which provides the z-averaged diffusion coefficient with real physical meaning, $\langle D \rangle_z$,

$$D_{\mathrm{app}}(q,w) = \langle D \rangle_z (1 + k_D w + C R_g{}^2 q^2). \tag{11}$$

where $k_D$ is the hydrodynamic virial coefficient and $C$ a coefficient depending on the slowest internal motion and polydispersity of the scattering particles. The hydrodynamic radius is calculated using the Stokes-Einstein equation

$$R_H = \frac{k_B T}{6\pi\eta \langle D \rangle_z}, \tag{12}$$

where $k_B$ is the Boltzmann constant, $T$ the temperature and $\eta$ the viscosity of the solvent.

An inverse Laplace transform of the autocorrelation function $g_1(t)$ provides the distribution of relaxation times, $\tau A(\tau)$,

$$g_1(t) = \int_{-\infty}^{\infty} \tau A(\tau) \exp(-t/\tau) \mathrm{d} \ln \tau, \tag{13}$$

which informs us about the polydispersity of the system.

## 4.2. Fluorescence Measurement and Solvent Relaxation Technique

### 4.2.1. Introduction

The term fluorescence was firstly introduced in a paper entitled 'On the Refrangibility of light' in 1852 by Stokes, where he originally called this phenomenon *dispersive reflexion*, but in a remark, he wrote '*I confess I do not like this term. I am almost inclined to coin a word and call the appearance fluorescence, from fluorspar, as the analogous term opalescence is derived from the name of a mineral.*' In this paper, he also demonstrated that the emission of light follows its absorption in fluorescence and that the emitted light has longer wavelength than the exciting light. Many publications have been devoted to the fluorescence since this time, but not only that, the fluorescence helps us nowadays to characterize polymer and biological systems.

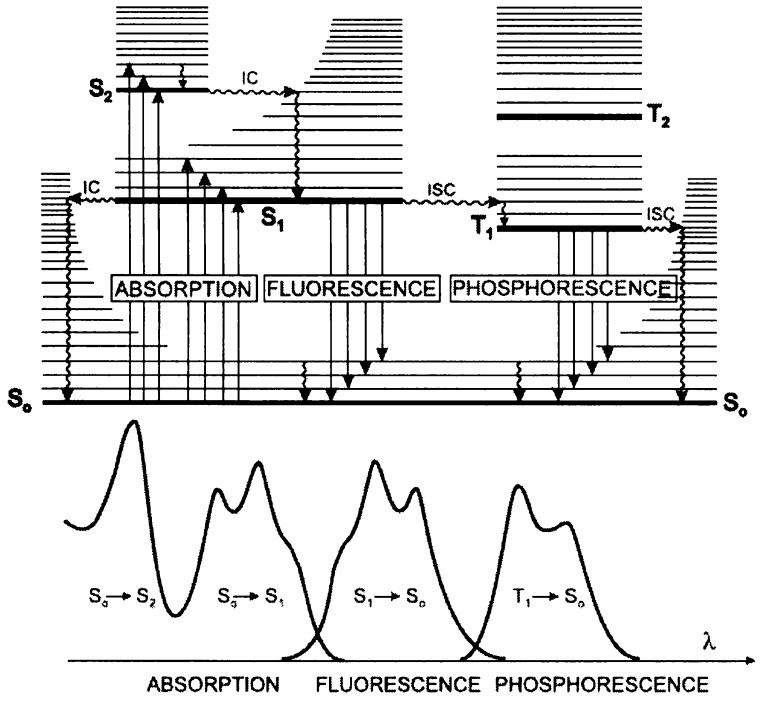


**Fig. 4.1.** Jablonski diagram. The picture was taken from: Valeur, B *Molecular Fluorescence: Principles and Applications*; VCH Verlag GmbH:Wiley, 2001.

### 4.2.2. Basic Principles of Fluorescence[42,43]

After a relatively rigid molecule, which has tendency to get rid of its redundant energy by emitting a photon, absorbs a quantum of light, it is excited from the ground state $S_0$ into one of the vibrational states of the level $S_n$, often $S_1$ (Fig. 2.1). According to the Franck-Condon principle, the absorption is so fast ($10^{-15}$ s) that the relative positions of nuclei do not change during the absorption process. The system relaxes very fast ($10^{-12}$ – $10^{-10}$ s) to the first excited state, whose lifetime corresponding to the timescale on which fluorescence takes place ranges from $10^{-10}$ to $10^{-7}$ s. After that the molecule returns to one of the vibrational levels of $S_0$ state by emitting a photon. Because fluorescence is a spin-allowed transition, it takes place on a timescale being much faster then in the case of phosphorescence, which is a spin-forbidden transition from the $T_1$ triplet state to the $S_0$ state.

When a large ensemble of molecules is considered, the decay rate of excited molecules can be expressed as in classical chemical kinetics by the following differential equation

$$-\frac{dN^*}{dt} = (k_r + k_{nr})N^*, \tag{14}$$

where $N^*$ is the number of molecules which are still in the excited state and $k_r$ or $k_{nr}$ are the rate constants for radiative or nonradiative deactivation, respectively. Since the fluorescence intensity, $I_F$, at specific time after excitation by a short pulse at time zero is proportional to the number of molecules still excited, we become $I_F$ after integration of eqn. (14)

$$I_F(t) = k_r N^* = k_r N_0^* \exp(-t/\tau_1), \tag{15}$$

where $N_0^*$ is the number of excited molecules at time 0 and $\tau_1$ the lifetime of the excited state $S_1$. Unfortunately, the fluorophores rarely exhibit single-exponential decays, so that the decay curves have to be fitted according to

$$I_F(t)' = B + \sum_{i=1}^{n} \alpha_i \exp\left(-\frac{t}{\tau_i}\right), \tag{16}$$

where $B$ is the correction factor to the background, $\alpha_i$ amplitudes and $\tau_i$ are lifetimes of the excited states. The deviations from the equation (15) are mainly caused by different localizations of the fluorophores, by excited state reactions or by solvent relaxation around the fluorescent probes.

### 4.2.3. Steady-State Fluorescence

Fluorescence or emission spectrum, $S(\lambda_F)$, reflects the distribution of probability of different transitions from the lowest vibrational level of $S_1$ state to the various vibrational levels of $S_0$ state. In practice, we measure the fluorescence intensity, $I_{EM}(\lambda_E,\lambda_F)$, which is proportional to the $S(\lambda_F)$ spectrum and to the intensity of absorbed light, $I_A(\lambda_E)$, fixed at a constant excitation wavelength,

$$I_{EM}(\lambda_E,\lambda_F) = k_p S(\lambda_F) I_A(\lambda_E), \tag{17}$$

where the proportionality factor $k_p$ depends in particular on the optical configuration of the fluorometer and the bandwidth of the monochromator. This equation can be rewritten using the Lambert-Beer law as

$$I_{EM}(\lambda_E,\lambda_F) = k_p S(\lambda_F) I_0(\lambda_E)\{1-\exp[-2.3\varepsilon(\lambda_E)lc]\} \cong$$

$$\cong 2.3 k_p S(\lambda_F) I_0(\lambda_E) A(\lambda_E), \tag{18}$$

where $I_0(\lambda_E)$ denotes the intensity of the incident light, $\varepsilon(\lambda_E)$ the molar absorption coefficient of the fluorophore at the wavelength $\lambda_E$, $l$ the optical path in the sample, $c$ the molar concentration of the fluorophore and $A(\lambda_E) = \varepsilon(\lambda_E)lc$ is the absorbance of the fluorescent probe. The eqn. (18) only confirms that the measured fluorescent intensity, $I_{EM}$, provides the fluorescent spectrum, $S$, in arbitrary units if the intensity of incident light is constant and fixed at certain wavelength. Moreover, the measured fluorescent signal depends linearly on the concentration of the fluorophore in the sample, provided that the concentration is low enough.

Unlike the emission spectra, the excitation spectra are measured by changing the excitation wavelength while the emission monochromator remains at a fixed position. We can see from the eqn. (18) that the intensity $I_{EM}$ is proportional to the absorption spectrum, $A(\lambda_E)$, so far the intensity of the incident light, *i.e.*, the lamp profile, is wavelength independent.

### 4.2.4. Time-Resolved Fluorescence

Measuring time-resolved fluorescent decays is in our case based on the *time-correlated single photon counting* (TCSPC) method.[42] It relies on the fact that the probability of detecting a single photon at the time $t$ after an exciting pulse is proportional to the fluorescence intensity at that time. In principle, when measuring decay curves, a sensitive

photomultiplier detects repeatedly the first emitted photon after the excitation pulse. After the photon is registered, the content of a memory channel corresponding to the time between the excitation pulse and the registration of the photon is increased by one. Sufficient amount of photons has to be detected (in our case 5000 at maximum) in order to obtain representative decay curves from recorded histograms.

Unfortunately, the pulse profile of a flash lamp or laser is not infinitively short, so that the observed fluorescence decay $R(t)$ is the convolution of the real fluorescence decay with the excitation profile, *i.e.*,

$$R(t) = \int_0^t L(t')D(t-t')\mathrm{d}t', \tag{19}$$

where $L(t')$ the intensity of the excitation pulse at the time $t'$ and $D(t\text{-}t')$ is the real fluorescent decay at the time $t\text{-}t'$ after the excitation. In order to estimate the function $D(t)$, a deconvolution procedure has to be carried out. It consists in minimizing numerically the expression

$$\chi^2 = \frac{1}{\upsilon}\sum_{i=1}^{N}\left(\frac{R(t_i) - R_c(t_i)}{\sigma_i}\right)^2, \tag{20}$$

where $\upsilon$ is the number of degrees of freedom, $R_c(t_i)$ is the fit of the function $R(t_i)$ obtained after convolution of $I(t)$' with $L(t)$ and $\sigma_i$ the standard deviation. From this follows that optimised parameters are $B$, $\alpha_i$ and $\tau_i$.

### 4.2.5. Solvent Relaxation[23,25,44,45]

#### *4.2.5.1. Introduction*

Whether we are able to observe solvent relaxation or not, in all cases, the fluorophore which participates in the solvent relaxation process must exhibit a large change of its dipole moment upon excitation and must be excited in a polar medium.

Although the absorption of light is very fast (see part 2.2), the electrons of the excited molecule do manage it to redistribute newly during this time, which results in an almost instantaneous change in the dipole moment. The surrounding polar solvent molecules react upon this change by their reorientation leading to the minimization of energy of the excited state.

If the polar medium is very viscous, the solvent molecules reorient slowly, so that the fluorophore emits its light mainly from the unrelaxed state (Fig. 2.2). On the contrary, in the nonviscous medium, the relaxation process is so fast that almost all registered photons come from the relaxed state. The steady-state fluorescence spectrum is in such a case red-shifted with respect to the spectrum of the fluorophore found in a very viscous medium.

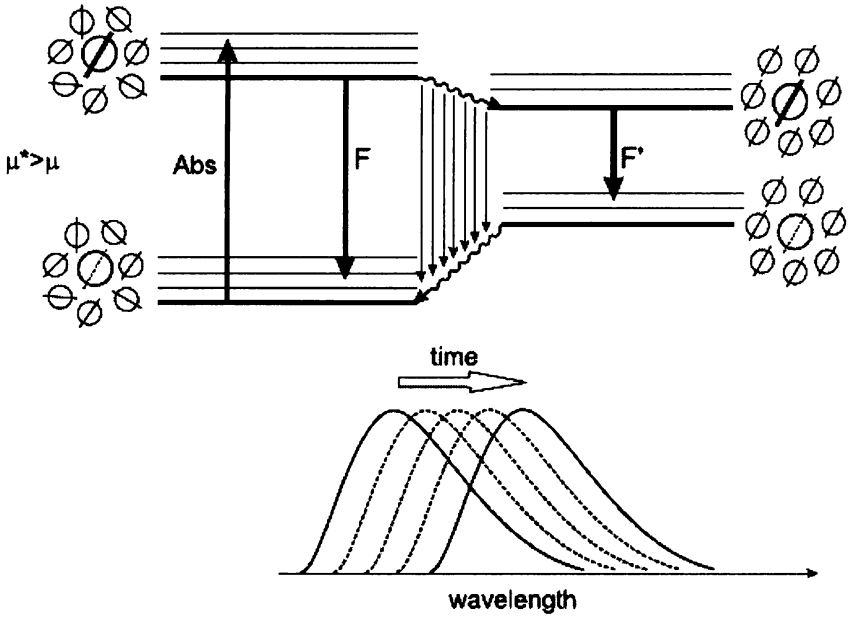


**Fig. 4.2.** Solvent relaxation around the dye molecules. The picture was taken from: Valeur, B *Molecular Fluorescence: Principles and Applications*; VCH Verlag GmbH:Wiley, 2001.

However, when the relaxation rate is comparable with the lifetime of the excited state, the fluorescence relaxation can be followed by the time-resolved fluorescence spectrometer and generation of time-resolved emission spectra (TRES) or time-resolved area normalized emission spectra (TRANES) is possible.

### *4.2.5.2. Generation of TRES and TRANES*

TRES together with TRANES, which can give us information about the nature of relaxation, and thus about our system studied, are determined using the so-called spectral reconstruction method.[46] It consists in the following few steps: (i) firstly, we have to measure decay curves for a set of wavelengths and decompose them as described in section 2.4; (ii) secondly, the steady-state spectrum, $S(\lambda,t)$, of the same system is required; (iii) thirdly,

TRES, $F(\lambda,t)$, at a given wavelength are calculated by the following normalization of the decomposed decays, $D(\lambda,t)$,

$$F(\lambda,t) = \frac{D(\lambda,t)S(\lambda,t)}{\int_0^\infty D(\lambda,t)\mathrm{d}t}; \tag{21}$$

(iv) finally, the obtained spectra are fitted in the wavenumber domain by the log-normal function, very well suitable for fitting of the emission spectra,

$$F_{\mathrm{fit}}(\omega,t) = h\exp\left\{-\ln(2)\left[\ln\left(\frac{1+\alpha}{\gamma}\right)\right]^2\right\} \text{ for } \alpha > -1$$

$$F_{\mathrm{fit}}(\omega,t) = 0 \text{ for } \alpha \leq -1, \tag{22}$$

$$\alpha = 2\gamma\frac{\omega-\omega_{\mathrm{p}}}{\Delta}, \tag{23}$$

where $F_{\mathrm{fit}}(\omega,t)$ denotes the fit of the time-resolved emission spectrum, $h$ the peak-height, $\gamma$ the asymmetry parameter, $\omega_{\mathrm{p}}$ is the peak position in the wavenumber domain and $\Delta$ the width parameter.

TRANES are then calculated by pure normalization of time-resolved emission spectra with the area under the spectrum at time zero. The presence of an isoemissive point in the TRANES suggests that the fluorescent probe under investigation is localized in two different environments.

#### *4.2.5.3. Microviscosity around the Dye Molecules*

The time-evolution of the peak maximum, determined as described at the above-mentioned part, reflects the mobility of the solvent molecules surrounding the excited fluorophore. The mobility itself or in other words solvation dynamics depends then on the frictional forces presented in the microenvironment, which are further related to the microviscosity near the dye molecule. The so-called correlation function, $C(t)$, allows us to fully describe the solvation dynamic occurring in the system

$$C(t) = \frac{\omega(\mathrm{peak},t)-\omega(\mathrm{peak},\infty)}{\omega(\mathrm{peak},0)-\omega(\mathrm{peak},\infty)} = \frac{\omega(\mathrm{peak},t)-\omega(\mathrm{peak},\infty)}{\Delta\omega}, \tag{24}$$

where $\omega(\mathrm{peak},t)$ indicates the peak position in the wavenumber domain at time $t$ after excitation and $\Delta\omega$ indicates the overall Stokes shift depending on the micropolarity around the dye molecules. The correlation function has the form of an exponential decay but only

rarely it can be fitted by a single-exponential function. Three or four exponential components are often needed to obtain a satisfying fit.

For our next considerations about the microviscosity inside the nanoparticles it is convenient to define the average relaxation time, $\tau_R$, as

$$\tau_R = \int_0^\infty C(t)\mathrm{d}t, \tag{25}$$

which can serve very well as a quantitative measure of the microviscosity around the dye. However, one has to bear in mind all the time that $\tau_R$ yields average information about the system only and that it is necessary to use the $C(t)$ function instead when thinking about the solvation dynamic processes.

#### *4.2.5.4. Full Width at Half Maximum*

Since the fluorescence deexcitation and the solvent relaxation can proceed on different timescales, it is useful to know whether we are able to follow the whole relaxation process with our equipment or not. Besides the time zero estimation (see the next part), the time-evolution of the full width at half maximum (FWHM) can help us to learn more about the extent of the observed solvent relaxation.

The estimation is based on the fact that the FWHM passes a pronounced maximum in inhomogeneous systems such as lipid bilayers or supercooled liquids as a function of time. This phenomenon is caused by the spatial distribution of solvent response times. When a sample is excited by a light pulse, individual fluorophores distributed in the system respond with different rate to changes in the local electric field. The inhomogeneity in the reorientation of solvent molecules around the dye molecules increases significantly immediately after the excitation. However, as the solvent shell of the fluorophores approaches equilibrium, the inhomogeneity starts to decrease after having reached its maximum.

This effect gives the origin for the method of checking whether the entire response or only a part of it was captured within the time-window of the experiment. Observing only an increase in the FWHM means that the solvent relaxation is slow and/or the lifetime of the excited state is short. On the contrary, very fast relaxation, which is beyond the resolution of the equipment used, results in observing only the decrease in the FWHM.

At the end it should be noted that such a complex behaviour of the FWHM is no more valid for homogenous solutions with low-molar-mass molecules, where the FWHM monotonously decreases with time.

#### *4.2.5.5. Time Zero Estimation*[47]

Whatever time-resolved spectrometer we use, the finite resolution of this equipment makes it impossible to record the emission spectrum at time zero after the absorption of light. However, the spectrum at time zero is needed, because without knowing the peak position at time zero, one cannot calculate the correlation function $C(t)$. In addition, the evaluation of the peak position at time zero can tell us more about the extent of the solvent relaxation that is beyond our resolution. Thus, a method enabling to reconstruct the emission spectrum at time zero has been elaborated.

The model assumes that polar absorption spectra are inhomogenously broadened due to the distribution of molecules over a range of local solvation environments and that the absorption spectra of two molecules residing in different microenvironments differ only by a frequency shift $\delta$. The homogenous broadening in a polar solvent is assumed to be the same as in a nonpolar solvent, which is valid without any inconvenience only then if the inhomogenous broadening is large (as it always is in a polar solvent) with respect to the homogenous broadening. The frequency absorption spectrum, $A_p(\nu)$, is thus given by the convolution of the absorption spectrum in a nonpolar solvent, $A_{np}(\nu)$, with the distribution of spectral shifts, $p(\delta)$,

$$A_p(\nu) \propto \int A_{np}(\nu - \delta)p(\delta)\mathrm{d}\delta. \tag{26}$$

The distribution of spectral shifts, $p(\delta)$, is supposed to be Gaussian

$$p(\delta) = \frac{1}{\sqrt{2\pi\sigma^2}}\exp\left[-\frac{(\delta-\delta_0)^2}{2\sigma^2}\right], \tag{27}$$

where $\sigma$ is the variance of the distribution and $\delta_0$ the average shift induced by the polar solvent. The unknown coefficients $\sigma$ and $\delta_0$ are determined from the eqn. (26) by an iterative procedure, provided that absorption spectra both in a polar and nonpolar solvent have been successfully measured.

Similar to the eqn. (26), the desired fluorescence spectrum at time zero, $F_p(\nu,\nu_{ex},t=0)$, can be expressed as

$$F_p(\nu,\nu_{ex},t=0) \propto \int A_{np}(\nu_{ex}-\delta)p(\delta)S_{np}(\nu-\delta)\mathrm{d}\delta, \tag{28}$$

where $S_{np}(\nu)$ stays for the emission spectrum in a nonpolar solvent. It means that the emission spectrum at time zero before any relaxation occurs can be reconstructed from the known emission and absorption spectra in a nonpolar solvent and from the absorption spectrum in a polar medium. To obtain these spectra need not to be always easy because of limited solubility of some probes in a nonpolar solvent.

Maroncelli *et al.* have shown that it is possible to further simplify the expression (28) if the fluorophores are excited near the absorption maximum, where almost no preferential selection of the solvation state occurs. The simplified equation has the form

$$\nu_p(t=0) \approx \nu_p(\text{abs}) - \nu_{np}(\text{abs}) + \nu_{np}(\text{em}), \tag{29}$$

where $\nu$ denotes the peak positions of the maximum and the subscripts *p* and *np* indicate polar or nonpolar medium, resp. When using this simplified equation, the deviations in determining the position of the maximum have been found not to exceed 50 $cm^{-1}$.

## 4.3. Atomic Force Microscopy Technique

Atomic force microscopy is a technique that directly visualises the surface of interest with relatively high resolution, which is of the order of $10^1$ nm in the vertical direction and $10^0$ nm in the horizontal direction. Surprisingly, this technique has been shown to be very useful when studying various properties of formed nanoparticles in solutions.

In this case, the sample has to be first deposited on a surface. Unfortunately, the deposited particles are deformed on the surface by strong interactions between the surface and the particles. Even though, their sizes seem to be proportional to those in the solution, and one can evaluate the particle size distribution.[48] However, when interpreting the results, one must never forget that the conditions in the solution and on the surface are entirely different, which can lead to the phenomena such as enhancement of the aggregation behaviour on the surface or preferential sorption of small particles.

The principle of the method is based on monitoring the interactions between a sharp, mostly silicon tip fastened on the cantilever and the coated surface. Depending on the form of the interaction between the tip and the surface, three modes have been developed.

(i) In the contact mode, the tip has a permanent contact with the surface through the liquid layer while the force between the tip and the sample remains constant. The image is reconstructed from the movement of the scanner. This mode exhibits a large resolution and a

satisfying speediness; however, the permanent contact of the tip with the sample can damage weak samples such as coated polymer particles.

(ii) Unlike the contact mode, the tapping mode is very often used in colloid science because the dangerous contact between the tip and the weak sample is considerably reduced by oscillation of the tip near its resonance frequency above the sample. Both the amplitude (20-100 nm) of oscillations and the force between the tip and the sample are kept constant while the position of the scanner is changed and recorded. The contact between the tip and the liquid layer covering the sample comes on near the bottom turning point only.

(iii) The principle of the non-contact mode is similar to the tapping mode; the only difference consists in the fact that the tip has neither a physical contact with the sample nor with the liquid layer above it. The amplitude of the cantilever does not exceed 10 nm, so that the interactions between the tip and the surface can only be confined to the van der Waals forces.

Beside the choice of an appropriate mode, one has to choose the surface that is to be coated correctly. Since the sizes of the self-assembled polymers are in the nanometer range, the surface should be flat on the same scale. From the experiments carried out in our group, freshly prepared mica seems to fulfil these requirements. It binds different types of polymers whatever charge they possess.[48-50]

# 5. Experimental Part

## 5.1. Equipment and Methods Used

**Light scattering measurements:** The light scattering equipment (ALV, Langen, Germany), which enables measuring both static and quasielastic light scattering, consists of a 633 nm He-Ne laser, an ALV CGS/8F goniometer, an ALV High QE APD detector and an ALV 5000/EPP multibit multitau autocorrelator. The measurements were carried out for polymer solutions with mass concentrations lying between 0.2 and 2 g/L at different angles ranging from 30° to 150° at 20°C. All the polymer samples were filtered through 0.45 μm Acrodisc filters after assuring that the solution did not contain dust particles.

Obtained static light scattering data were treated by the Berry method according to the eqn. (6). Refractive index increments of PCL-PEO in water were calculated as the weighted average of literature data for PCL and PEO.[51,52] Because of the very low solubility of PCL in water, we took the literature values for PCL in THF[52] and recalculated them to water, assuming that the difference between increments in two solvents equals the difference of refractive indexes of the solvents.[40] The same approximation was employed for the calculation of increments of PCL-PEO in THF/water mixtures, using the literature data on the refractive index dependence on the composition of THF/water mixtures.[53]

The evaluation of the dynamic light scattering data is based on the analysis of the measured normalized autocorrelation function, $g_2(t)$, related to the electric field autocorrelation function, $g_1(t)$. The distribution of relaxation times, which can be expressed as the inverse Laplace transform of the $g_1(t)$ function (see section 4.1.2), is obtained with the help of the constrained regularization algorithm (CONTIN). The fit of $g_1(t)$ function according to eqn. (9) provides the apparent diffusion coefficient, $D_{app}$.

**Steady-state fluorescence measurements:** All steady-state excitation and emission spectra acquisitions were performed on the Fluorolog 3 fluorometer (model FL3-11, Jobin Yvon Inc., Edison, NJ, USA) equipped with a xenon-arc lamp at room temperature. The spectra were collected in 1 nm intervals with both excitation and emission monochromators fixed at 2 nm bandwidths.

**Time-resolved fluorescence measurements:** The time-correlated single photon counting method[42] was used for measurements of fluorescence decays, which were recorded at different wavelengths ranging from 400 to 540 nm by IBH 5000U time-resolved fluorometer (IBH, Glasgow, UK), equipped with an IBH laser diode NanoLED 11 (370 nm peak wavelength, 80 ps pulse width, 1 MHz maximum repetition rate) and cooled Hamamatsu R3809U-50 microchannel plate photomultiplier. Data was collected in 8192 channels (14 ps per channel) until the peak value reached 5000 counts. A 399 nm cut-off filter eliminated the scattered light. The recorded decays were deconvoluted and further fitted to 2 or 3 exponential functions by using the Marquardt-Levenberg non-linear least squares method. The $\chi^2$ values close to 1.0 and random distribution of residuals indicated good fit.

TRES or TRANES, respectively, were reconstructed by the spectral reconstruction method as described in section 2.5.2. The time zero was calculated using the simplified equation (29), *i.e.*, on the basis of determining maximum positions of both absorption and fluorescence spectra.

**UV-Vis absorption measurements:** UV-Vis absorption spectra were recorded with 1 nm increment in 1 cm quartz cuvettes using a Perkin-Elmer Lambda 19 UV-Vis spectrometer.

**Atomic force microscopy measurements:** Atomic force microscopy measurements were carried out in the tapping mode under ambient conditions using a commercial scanning probe microscope, Digital Instruments NanoScope dimensions 3, equipped with a Nanosensors silicon cantilever with typical spring constant 40 N $m^{-1}$. The solution with nanoparticles was deposited on a freshly peeled out mica surface (flogopite, theoretical formula $KMg_3AlSi_3O_{10}(OH)_2$, Geological Collection of Charles University in Prague, Czech Republic) by a fast dip coating in a dilute PCL-PEO solution (*w* ca. $10^{-2}$ g $l^{-1}$). After evaporation of water, the samples for AFM were dried in vacuum oven at ambient temperature for ca. 5 hours.

## 5.2. Materials

**Copolymer samples**: Three PCL-PEO polymers differing in the length of the PCL block, all with the polydispersity index less than 1.4, were purchased from Aldrich. Precise characteristics of the polymers are contained in the table 5.1.

**Tab. 5.1.** Characteristics of used PCL-PEO samples.

| | PCL | | PEO | |
|---|---|---|---|---|
| **Sample** | **$M_w$/g/mol** | **N(PCL)** | **$M_w$/g/mol** | **N(PEO)** |
| PCL(5)-PEO | 5000 | 44 | 5000 | 114 |
| PCL(13)-PEO | 13000 | 114 | 5000 | 114 |
| PCL(32)-PEO | 32000 | 281 | 5000 | 114 |

**Solvents**: Tetrahydrofuran, THF, luminescence spectroscopic grade, and deionised water were used as solvents.

**Fluorescent probes**: PRODAN, 6-propionyl-2-(dimethylamino)naphthalene, and LAURDAN, 6-lauroyl-2-(dimethylamino)naphthalene, were purchased from Molecular Probes (Eugene, Oregon).

## 5.3. Preparation of Nanoparticles

All the PCL-PEO nanoparticles studied in this work were prepared in the following way: Variable amount of the polymer, *i.e.*, 9, 15 or 30 mg, respectively, was added to 3 ml THF/water mixtures, where the content of water changed from 0 to 20 vol.%. In order to dissolve the polymer completely in the mixtures, the solution was being shaken overnight. After that the polymer solutions were added drop-by-drop to 7 ml of water under vigorous stirring. The rest of THF was removed by dialysis against pure water, which was changed several times.

## 5.4. Incorporation of Fluorescence Probes

All fluorescence measurements were carried out with PCL(5)-PEO nanoparticles. They were prepared from 90 vol.% THF with the concentration of the polymer in the initial solvent $w_i$ = 5 mg/ml and the concentration in the final aqueous solution $w_f$ = 1.55 mg/ml. We took then 0.8 ml of the aqueous polymer solution and solubilized into it 26 μl of the 0.2 mM methanol solution of PRODAN or 10 μl of the 0.52 mM methanol solution of LAURDAN, respectively. After that, we added, under vigorous stirring, a varying amount of water and THF, so that the final volume of the solution always reached 2 ml and the content

of THF changed from 0 to 30 vol. % with 10 % step in the case of PRODAN and from 0 to 50 vol. % with 10 % step in the case of LAURDAN. Finally, the samples were let to equilibrate and measured primarily the next day.

# 6. Results and Discussion

## 6.1. Characterization of Aggregates in the Initial Solvent

I have already mentioned in the section 3.1.1. that the hydrophobic PCL block makes it impossible to dissolve PCL-PEO with more than 19 PCL units directly in water. We tried thus to find an organic solvent in which both the PCL and PEO block would be sufficiently soluble. Experiments on PCL-PEO with short PCL block carried out recently by Vangeyte *et al.*[7] led us to the idea to use tetrahydrofuran, THF, as the initial organic solvent. While THF is a very good solvent for the PCL block, the PEO block exhibits rather limited solubility in THF. We assumed therefore that addition of small amount of water into THF (THF is miscible with water) could improve the solubility of PCL-PEO samples (see section 5.1.) in THF because PEO block is hydrophilic.

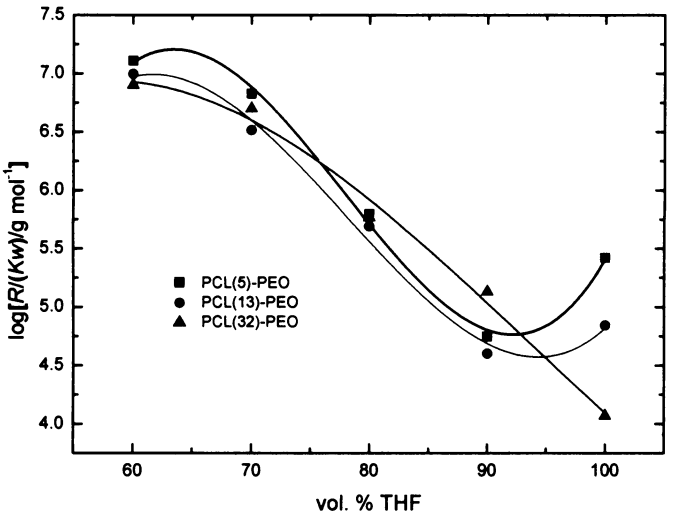


**Fig. 6.1.** The logarithm of the excess Rayleigh ratio, $\Delta R$, divided by $Kw$, proportional to the apparent molar mass, $M_w^{app}$, as a function of the THF/water ratio in volume % for all three copolymers differing in the length of the PCL block.

In order to test this hypothesis, we applied SLS and measured the dependence of the ratio $\Delta R/Kw$, which is roughly proportional to the molar mass of aggregates that scatter light (eqn.2 in section 4.1.1.) and is consequently called the apparent molar mass, $M_w^{app}$, on the content of water (in vol.%) in the initial THF/water mixed solvent (see Fig. 6.1). One can see that $M_w^{app}$ strongly depends on the amount of water in THF for all three copolymers. The

dependences for PCL(5)-PEO and PCL(13)-PEO pass a pronounced minimum near 90 vol.% THF/water mixture, which corresponds to the region where the polymers form the smallest aggregates. In other words, THF/water mixture containing ca. 10% of water is the best solvent for PCL(5)-PEO and PCL(13)-PEO. On the contrary, very long PCL chain of the PCL(32)-PEO polymer results in the monotonous increase of the apparent molar mass with the decrease of THF/water ratio.

Therefore, we were able to improve the solubility of PCL-PEO by adding water into THF solely for PCL(5)-PEO and PCL(13)-PEO, whose PCL/PEO mass ratio is still not so high that the solubility of the whole block-copolymer is controlled practically by the PCL block only.

## 6.2. Characterization of Aggregates in Pure Water

### 6.2.1. Dependence on the THF/water Ratio

In the next step, we wanted to find whether the sizes of aggregates found in THF/water mixtures correlate to those in water, *i.e.*, whether the properties of the initial aggregates, such as molar masses, hydrodynamic radii or radii of gyration, are proportional to the properties of the nanoparticles existing in water and being formed from the initial aggregates during addition of the polymer solution into water.

Our first attempts to dialyse THF/water polymer solution stepwise into pure water were not successful because the polymer solution aggregated relatively fast after the beginning of the dialysis. This behaviour has been already described for shorter PCL-PEO copolymers by Vangeyte *et al.*[7], and can be thus extended to PCL-PEO with longer PCL chain as well. We were thus forced to choose the preparation protocol described in the section 5.3., *i.e.*, to add the polymer solution drop-by-drop into water, which was vigorously mixed, and to dialyse the solution afterwards. This procedure gained representative and satisfying results.

As one of our goals was to prepare relatively monodisperse particles, we firstly evaluated distributions of relaxation times, $\tau A(\tau)$, which helped us to reveal size distributions of particles present in the system, for water containing nanoparticles formed from THF/water mixtures differing in the THF/water ratio. The distributions of relaxation times (see Fig. 6.2.) really suggest that the properties of particles found in water may have direct relationship to

the characteristics of the initial aggregates. The polydispersity of particles formed from 80, 70 and 60 vol.% THF is for all three copolymers very high and the particle-sizes reach from ones to thousands of nanometres. On the other hand, rather monodisperse particles are formed from 90 or 100 vol.% THF, respectively, with averaged sizes considerable smaller than in the previous case. The same trend concerning particle-sizes (molar masses) can be seen from Fig. 6.1, although one would need precise values for detailed comparison.

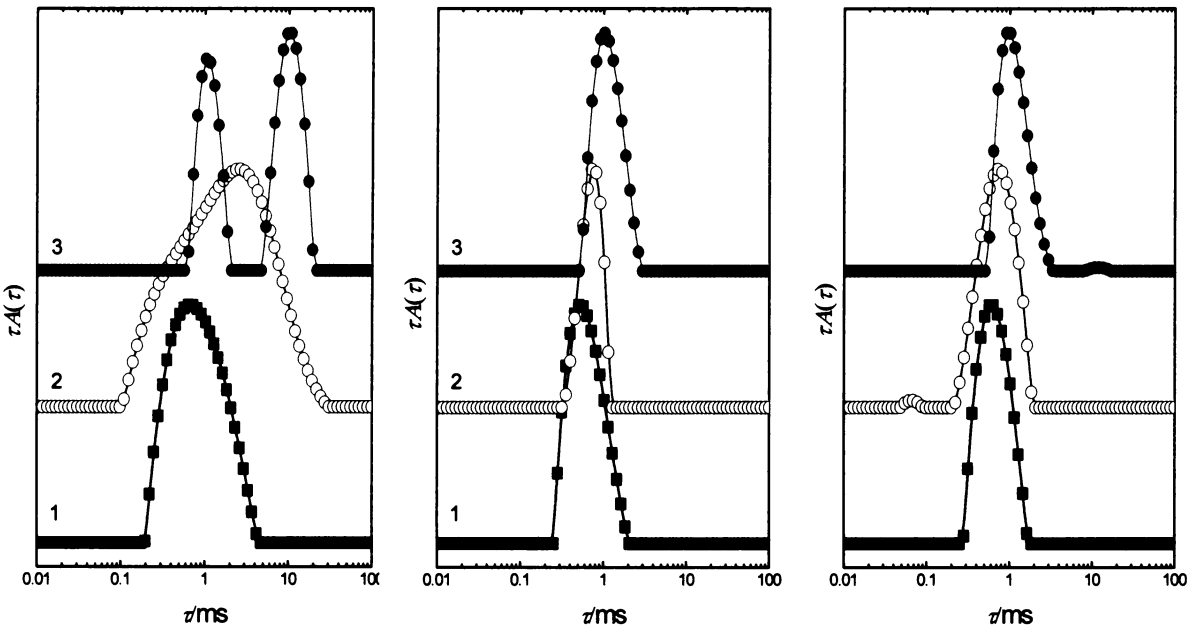


**Fig. 6.2.** The distributions of relaxation times measured at 90° for (1) PCL(5)-PEO, (2) PCL(13)-PEO and (3) PCL(32)-PEO. The particles were prepared from 80 vol.% THF (on the left), 90 vol.% THF (in the middle) and pure THF (on the right). The distributions for particles coming from 70 and 60 vol.% THF are very broad and similar to those prepared from 80 vol.% THF.

These precise values are accessible by means of static and quasielastic light scattering. Since the particle-sizes approached in some cases 200 nm in diameter, we chose the Berry plot, which is more reliable for larger particles, instead of the frequently used Zimm plot for the evaluation of data provided by SLS. By fitting the experimental data linearly in the Berry plot and extrapolating them to the zero angle and to the zero concentration, we obtained weight-averaged molar masses, $M_w$, and radii of gyration, $R_g$, of the particles transferred into water. As all the Berry plots are similar to each other, we present one demonstrative plot only (see Fig. 6.3). The same extrapolation procedure has to be carried out to obtain diffusion coefficients or hydrodynamic radii, $R_H$, of the nanoparticles (see section 4.1.2 and a representative plot in Fig. 6.4).

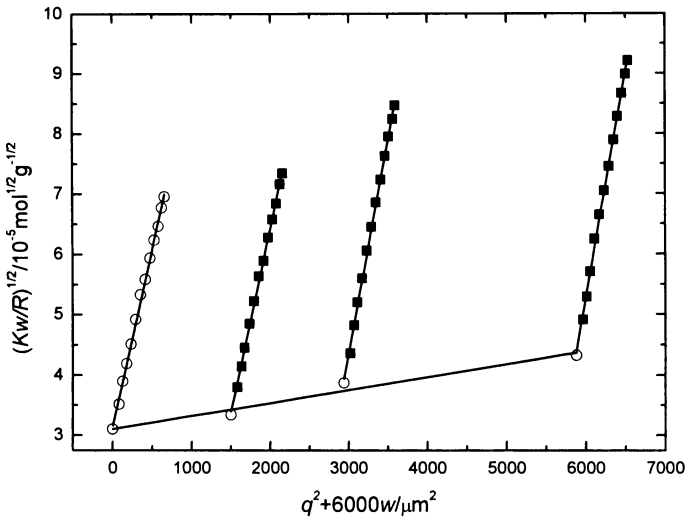


**Fig. 6.3.** A typical Berry plot for PCL(32)-PEO transferred into water from 90 vol.% THF/water mixture, where the mass concentration of the polymer was 10mg/ml. The polymer-concentrations in the measured samples were 0.25, 0.49 and 0.98 g/ml.

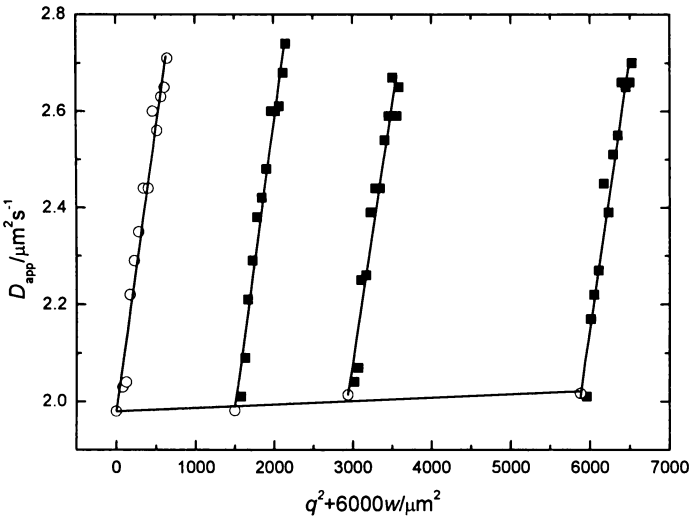


**Fig. 6.4.** A dynamic Zimm plot for PCL(32)-PEO particles in pure water. We took for the measurement of diffusion coefficients the same samples as in Fig.6.3.

The data that provided us LS are summarized in tabs. 6.1 and 6.2. The tables contain in addition the particle-aggregation numbers, $Z$, calculated by dividing the weight-averaged molar mass of the whole particle, $M_w$, by the known number-averaged molar mass of the polymer, the ratio $R_g/R_H$ and the effective density of the particle, $\rho_{eff}$, which can be calculated from $M_w$ and $R_H$ according to

$$\rho_{\text{eff}} = \frac{3M_w}{4\pi N_A R_H^{\ 3}}, \tag{30}$$

where $N_A$ is the Avoggadro's number. We *a priori* assume that the particle has spherical shape. As obvious from Fig. 6.2, the polydispersity of the particles prepared from 80 vol. % THF is so high that the averaged values would not tell us a lot. Hence, we present only results for particles coming from 90 vol.% and pure THF.

**Tab. 6.1.** Weight-averaged molar masses, $M_w$, aggregation numbers, Z, radii of gyration, $R_g$, hydrodynamic radii, $R_H$, ratios $R_g/R_H$ and effective densities, $\rho_{\text{eff}}$, for nanoparticles prepared from 90 vol.% THF/water mixture, where the concentration of the polymers was 10mg/ml.

| Sample | $M_w$/g/mol | $Z$ | $R_g$/nm | $R_H$/nm | $R_g/R_H$ | $\rho_{\text{eff}}$/g cm$^{-3}$ |
|---|---|---|---|---|---|---|
| PCL(5)-PEO | (4.16 ± 0.04)10$^7$ | 4159 ± 42 | 42.3 ± 0.8 | 46.8 ± 0.7 | 0.90 ± 0.03 | 0.16 ± 0.01 |
| PCL(13)-PEO | (6.56 ± 0.08)10$^7$ | 3646 ± 44 | 53.2 ± 0.9 | 53.4 ± 0.2 | 1.00 ± 0.02 | 0.17 ± 0.00 |
| PCL(32)-PEO | (1.00 ± 0.03)10$^9$ | 27108 ± 699 | 105.6 ± 1.1 | 110.2 ± 1.2 | 0.96 ± 0.02 | 0.30 ± 0.02 |

**Tab. 6.2.** Weight-averaged molar masses, $M_w$, aggregation numbers, $Z$, radii of gyration, $R_g$, hydrodynamic radii, $R_H$, ratios $R_g/R_H$ and effective densities, $\rho_{\text{eff}}$, for nanoparticles prepared from pure THF with the polymer concentration of 10mg/ml.

| Sample | $M_w$/g/mol | $Z$ | $R_g$/nm | $R_H$/nm | $R_g/R_H$ | $\rho_{\text{eff}}$/g cm$^{-3}$ |
|---|---|---|---|---|---|---|
| PCL(5)-PEO | (5.23 ± 0.03)10$^7$ | 5225 ± 33 | 51.4 ± 2.3 | 51.7 ± 1.1 | 0.99 ± 0.07 | 0.15 ± 0.01 |
| PCL(13)-PEO | (5.65 ± 0.09)10$^7$ | 3138 ± 47 | 60.4 ± 0.9 | 57.7 ± 1.0 | 1.05 ± 0.03 | 0.12 ± 0.01 |
| PCL(32)-PEO | (6.94 ± 0.10)10$^8$ | 18743 ± 261 | 88.9 ± 0.7 | 96.0 ± 0.5 | 0.93 ± 0.01 | 0.31 ± 0.01 |

Provided that the properties of the initial aggregates and the particles existing in water correlate with each other, one would expect, based on Fig. 6.1 valid for the initial aggregates, that (1) the final particles formed from PCL(5)-PEO will be larger when pure THF instead of 90 vol.% THF is used as the initial solvent, (2) the final nanoparticles formed from PCL(32)-PEO will be smaller when dissolving the polymer in pure THF because the molar mass of the initial PCL(32)-PEO aggregates continuously decreases as the content of water in THF is lowered, (3) the final particles that were formed from PCL(13)-PEO dissolved in 90 vol.% THF or pure THF, respectively, will be the least different from each other. This trend can be really read out from tabs. 6.1 and 6.2. While the relative changes in molar masses reach 25.7

% or even 44.1% for PCL(5)-PEO or PCL(32)-PEO, respectively, the relative change in $M_w$ for PCL(13)-PEO is equal to only 16.4%. The fact that the properties of the initial and final aggregates correlate with each other quite well suggests that the final particles present in water may be formed by the quenching mechanism. Under this term we understand that the aggregates that are present in the initial solvent under equilibrium freeze during the addition of the polymer solution into water. Without aggregating, these particles can exist in water for a long time; however, they are no more in equilibrium.

### 6.2.2. Dependence on the Polymer Concentration in the Initial Solvent

Another factor that influences the particle dimensions is the concentration of the polymer in the initial THF/water mixture. We thus decreased the polymer concentration to 5 and 3 mg/ml. With respect to the minimum in the molar mass for PCL(5)-PEO and PCL(17)-PEO in ca. 90 vol.% THF, we decided to use the 90 vol.% THF/water mixture as the initial solvent for all three polymers. The rest of the preparation protocol remained as it was. The results are summarised in tabs. 6.3 and 6.4.

**Tab.6.3.** Characteristics for nanoparticles prepared from 90 vol.% THF/water mixtures. The concentration of the polymer in the initial solvent was 5mg/ml.

| Sample | $M_w$/g/mol | $Z$ | $R_g$/nm | $R_H$/nm | $R_g/R_H$ | $\rho_{eff}$/g cm$^{-3}$ |
|---|---|---|---|---|---|---|
| PCL(5)-PEO | $(1.41 \pm 0.02)10^7$ | 1408 ± 20 | 34.6 ± 1.4 | 36.8 ± 1.4 | 0.94 ± 0.07 | 0.11 ± 0.01 |
| PCL(13)-PEO | $(3.91 \pm 0.08)10^7$ | 2173 ± 47 | 47.8 ± 1.5 | 47.8 ± 1.5 | 1.00 ± 0.06 | 0.14 ± 0.02 |
| PCL(32)-PEO | $(2.93 \pm 0.03)10^8$ | 7930 ± 90 | 64.0 ± 0.7 | 70.0 ± 0.6 | 0.91 ± 0.02 | 0.34 ± 0.01 |

**Tab.6.4.** Characteristics for nanoparticles prepared from 90 vol.% THF/water mixtures. The concentration of the polymer in the initial solvent was 3mg/ml.

| Sample | $M_w$/g/mol | $Z$ | $R_g$/nm | $R_H$/nm | $R_g/R_H$ | $\rho_{eff}$/g cm$^{-3}$ |
|---|---|---|---|---|---|---|
| PCL(5)-PEO | $0.94.10^7$ | 935 | 37.8 | 35.1 | 1.08 | 0.09 |
| PCL(13)-PEO | $(3.53 \pm 0.06)10^7$ | 1960 ± 34 | 46.4 ± 1.6 | 44.2 ± 1.4 | 1.05 ± 0.07 | 0.16 ± 0.02 |
| PCL(32)-PEO | $(1.06 \pm 0.02)10^8$ | 2873 ± 45 | 47.8 ± 1.1 | 52.4 ± 1.2 | 0.91 ± 0.04 | 0.29 ± 0.03 |

The particles are rather monodisperse with narrow distributions of relaxation times similar to those for particles prepared from 90 vol. % THF with the concentration 10mg/ml (see Fig. 6.2 in the middle). As the polymer-concentration in the 90 vol. % THF/water mixtures is lowered, the sizes of final particles decrease. It can be in part the consequence of the fact that the average distance among the particles increases after dilution, so that the probability of the particle-aggregation is then during the addition of the polymer solution into water lower. The most pronounced changes in particle-sizes are evident for the PCL(32)-PEO particles, whose aggregation number changes from ca 2.7 $10^4$ to only 2.9 $10^3$. It is therefore slightly surprising that the effective density of the particles remains almost unchanged after dilution.

Vangeyte *et al.*[7] investigated the influence of the polymer-concentration on the particle-sizes as well. They found, unlike our experiments, that the hydrodynamic radii of the observed particles increase from 22 nm to 31 nm with the decrease in concentration from 1 to 0.1 mg/ml. However, they prepared the particles from pure THF and the PCL block had only 16 monomer units, which could explain the different behaviour.

### 6.2.3 Particle-characteristics

As we can see from tabs. 6.1–6.4, the sizes of the final nanoparticles are too large and their aggregation numbers are too high to assume that they have simple core/shell micellar structure. For comparison, Winnik *et al.*[54] or Xu *et al.*[10] reported that diblock copolymers of polystyrene-*block*-poly(ethylene-oxide) with molar masses from 8500 to 50800 g/mol formed the core/shell micelles with hydrodynamic radii ranging from 10 to 23 nm and aggregation numbers from 350 to 1850. On the contrary, hydrodynamic radii about 50 nm and aggregation numbers about 5000, *i.e.*, values comparable to those obtained in this study were reported by Eisenberg *et al.*[55] for vesicles formed by asymmetrical polystyrene-*block*-poly(acrylic acid) with molar masses 32000 and 4000 g/mol for polystyrene and poly(acrylic acid) blocks, respectively. This comparison suggests that the particles could have the vesicle-like structure.

This assumption is further supported by the ratios $R_g/R_H$ that are close to the theoretical value for the hollow sphere, $R_g/R_H = 1$. The deviations of our light scattering data from this predicted value could be caused by the polydispersity and finite wall thickness of the formed vesicles.

The relatively low averaged effective densities of the nanoparticles are in agreement with the vesicle-formation, too. Such low values indicate that a considerable part of the nanoparticle volume, comprising probably the cavity of the core as well, is filled with water.

On the other hand, vesicles described by Eisenberg *et al.*[55] exhibited broad size distributions while the wall-thickness remained constant. However, these particles were in equilibrium during the whole process of their preparation, unlike the nanoparticles presented here, which were in equilibrium in the initial solvent only.

### 6.2.4. AFM Imaging of PCL-PEO Nanoparticles

In order to confirm the formation of vesicles by another method than light scattering, we applied the atomic force microscopy, AFM, by means of which the nanoparticles can be directly visualised when deposited on the freshly peeled-off mica surface (see the experimental section 5.1). Even though the thermodynamic conditions on the surface are completely different from those in the solution, which can lead to aggregation of the particles on the surface or preferential sorption of small particles during deposition, the particle-sizes appear to be proportional to those in the solution. The deposited particles are often pancake-deformed with a horizontal diameter considerably larger than the vertical one. From a lot of studies it follows that the vertical diameter can serve as a rough estimation of the micellar core.

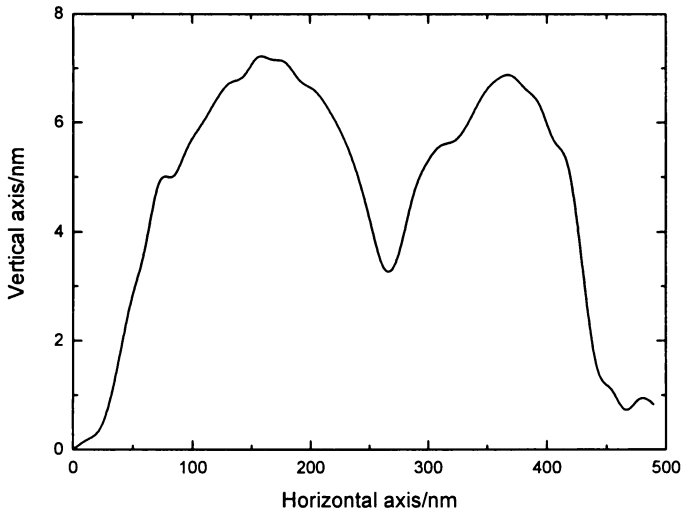


**Fig. 6.5.** The profile of two aggregating nanoparticles from Fig. 6.6.

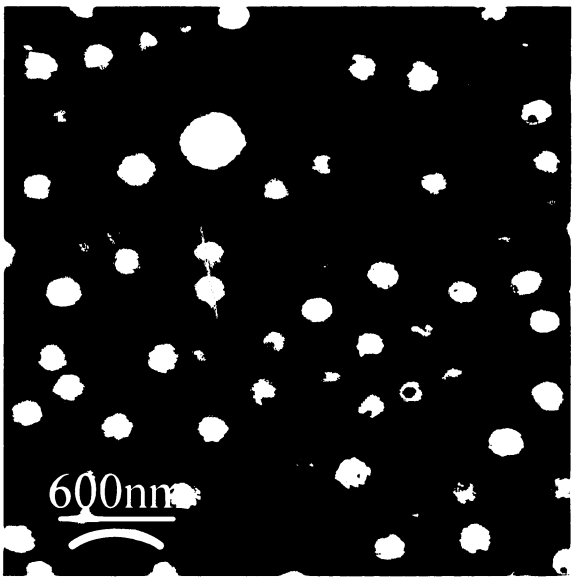


**Fig. 6.6.** AFM scan of the PCL(5)-PEO nanoparticles prepared from 90 vol.% THF, in which the concentration of the polymer was 5 mg/ml. The picture was obtained in the tapping mode. The blue line denotes the position where the profile was measured.

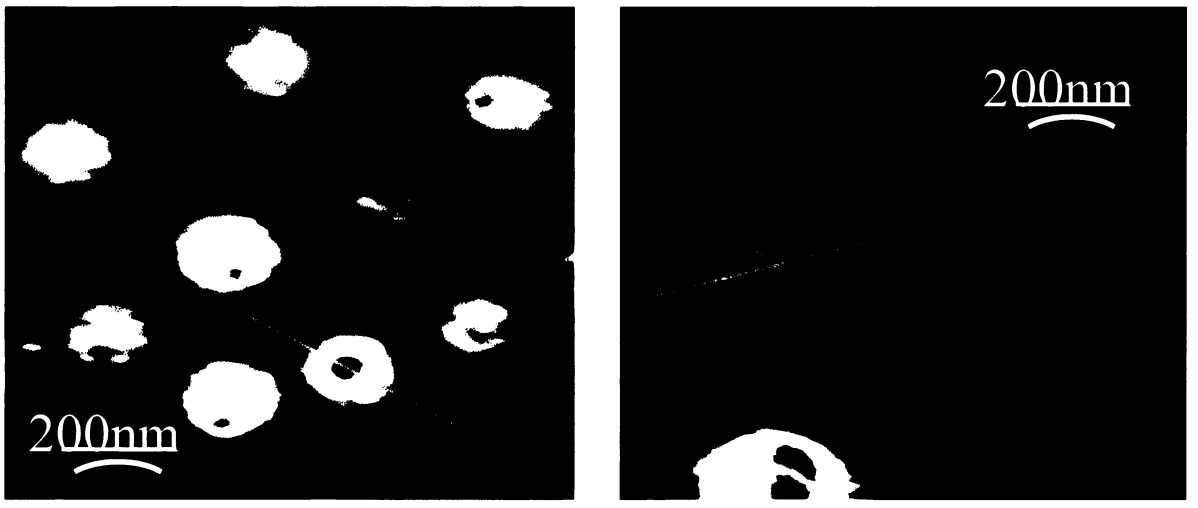


**Fig. 6.7.** (A) AFM scan of the PCL(5)-PEO nanoparticles and (B) AFM scan of the PCL(32)-PEO nanoparticles. The particles were prepared from 90 vol.% THF, in which the concentration of the polymer was 5 mg/ml. The blue line denotes the position where the profile was measured.

On the AFM scans, we observed a rather high tendency of the PCL-PEO particles to aggregate on the mica surface during the deposition. The aggregation is probably caused by the corona PEO block, whose aggregative behaviour is well known. Even though, we were able to catch nonaggregated particles on our AFM scans by diluting the aqueous polymer solution to the concentration of 0.01 g/l. Nevertheless, some of the particles can be seen jointed together after the dilution as well (see Figs. 6.5 and 6.6).

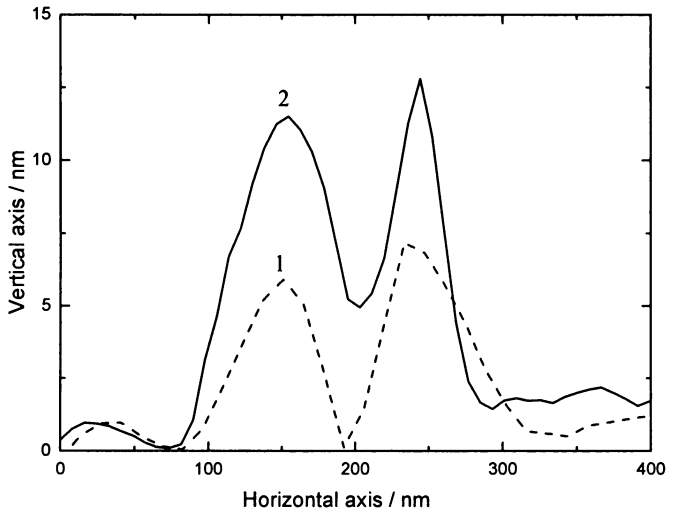


**Fig. 6.8.** (1) Profile of the particle displayed in Fig. 6.7 (A). (2) Profile of the particle displayed in Fig. 6.7 (B).

Most of the particles that we observed were ring-shaped (see the profiles in Fig. 6.8 and AFM scans in Fig. 6.7, the scan for PCL(13)-PEO is not shown here), with a hollow in the centre. The presence of the hollow in the centre of the deposited particles supports the assumption that vesicles were formed instead of micelles, since the presence of the hollow can be explained as a result of the collapse of the vesicle wall after the evaporation of water. The radius of the nanoparticles prepared from 90 vol.% THF, where the concentration of the polymer was 5 mg/ml, approached 110 nm for both the PCL(5)-PEO and PCL(32)-PEO polymers while the heights reached 6 nm for PCL(5)-PEO and 12 nm for PCL(32)-PEO (see Fig. 6.8). Unfortunately, we cannot estimate the thickness of the vesicle wall purely on the basis of AFM measurements because the dimensions of the crater depend on how much the vesicle wall burst after the evaporation of water.

### 6.2.5. Scaling Relations

Until now we were in particular interested in how the sizes of the nanoparticles depend on their concentration in the initial solvent or how the particle-sizes change with the composition of the THF/water mixtures. However, we have not yet dealt with the question how the varying length of the PCL block influences the particle-sizes and/or aggregation numbers, of the nanoparticles, $Z$.

From the theory,[56,57] it is well known that the aggregation numbers, $Z$, and hydrodynamic radii, $R_H$, of the micelles that are found in equilibrium scale according to $Z \approx N_{CL}^{\kappa}$ and $R_H \approx N^{\mu}$, where $N_{CL}$ is the number of CL units in the PCL-PEO polymer, $N$ the overall degree of polymerisation, $N = N_{CL} + N_{EO}$, and $\kappa$ and $\mu$ are theoretical exponents whose values depend both on the type of the polymer and the solvent.

If the thermodynamic state of the diblock copolymer corresponds to the weak segregation limit, WSL, both the blocks form the Gaussian coil with large interfacial thickness and the dimensions of the aggregates follow the scaling relations with $\kappa$ and $\mu$ equal to 0.5 and 0.5, resp. In the so-called strong segregation limit, SSL, with $\kappa = 1$ and $\mu = 2/3$, nearly pure microdomains of A and B blocks, where A indicates the core-forming block and B the shell-forming, are developed. When the interface is completely occupied by A-B junctions so that there is no place to incorporate more chains or the chains are fully stretched, new regime, namely super strong segregation limit, SSSL, with $\kappa = 2$ and $\mu = 1$, was reached. It is worth noting that for the crew-cut micelles, whose size is approximately the same as the size of its core, the same scaling relations were predicted as for the SSL while the amphiphile micelles, which are characterised by large Flory-Huggins interaction parameters $\chi_{A\text{-}B}$ and $\chi_{A\text{-}Solvent}$, follow the same scaling relations as A-B diblock copolymers found in the SSSL. Finally, $\kappa = 4/5$ and $\mu = 3/5$ relates to hairy micelles, which have the core negligibly small in comparison with the size of the shell.

We have already shown[9] that the PCL-PEO nanoparticles prepared from 90 vol.% THF in one particular concentration regime surprisingly follow the scaling relation for hairy or crew-cut micelles. In this study, we wanted to find whether the particles fulfil the same scaling relation under different concentration of the polymer in the initial solvent as well.

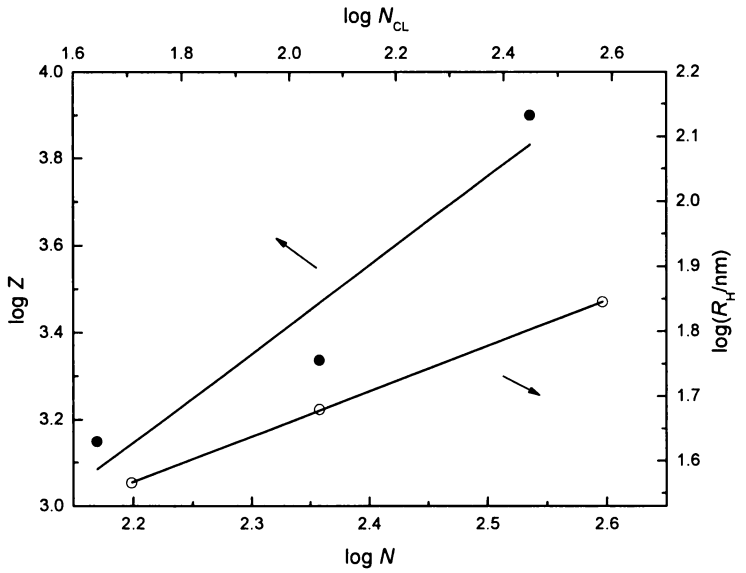


**Fig. 6.9.** Logarithm of the aggregation number, Z, of PCL-PEO particles as a function of the logarithm of the number of PCL units in PCL-PEO, $N_{CL}$, and logarithm of the hydrodynamic radius, $R_H$, of PCL-PEO particles as a function of the overall degree of polymerisation, $N$. The concentration of the polymer in the initial solvent was 3mg/ml.

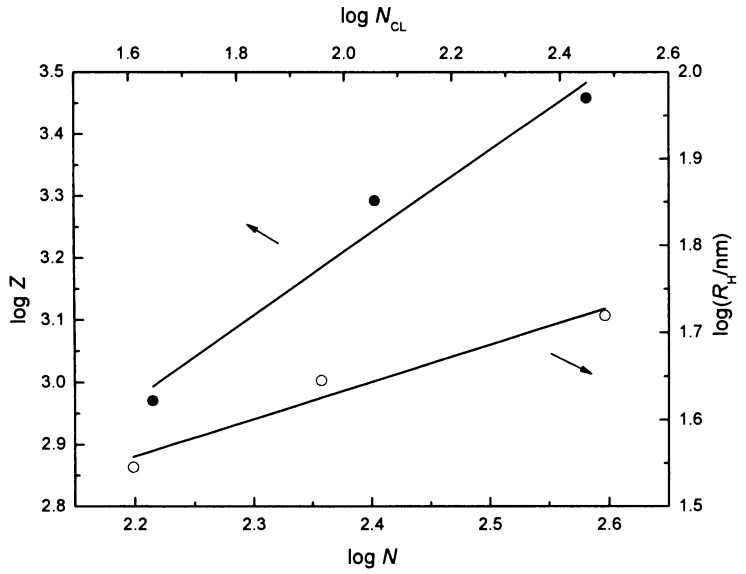


**Fig. 6.10.** Logarithm of the aggregation number, Z, of PCL-PEO particles as a function of the logarithm of the number of PCL units in PCL-PEO, $N_{CL}$, and logarithm of the hydrodynamic radius, $R_H$, of PCL-PEO particles as a function of the overall degree of polymerisation, $N$. The concentration of the polymer in the initial solvent was 5mg/ml.

The fit of the data obtained for the particles prepared from 90 vol.% THF with the concentration of the polymer 3 mg/ml, yielded $\kappa = 0.61$ and $\mu = 0.43$ with the correlation coefficients 0.99 and 0.98, resp. (see Fig. 6.9 and also tab. 6.4). These exponents are very close to those predicted for WSL and relatively close to the coefficients valid for the hairy micelles. The increase of the polymer concentration in the initial solvent to 5 mg/ml leads to $\kappa = 0.92$ and $\mu = 0.70$ with the correlation coefficients 0.96 and 1.0, resp (see Fig.6.10). These exponents fit quite well those predicted for SSL and crew-cut micelles and are in good agreement with the coefficients that we obtained in our earlier study[9] (that is no coincidence because both the concentrations regimes have very close to each other). On the other hand, when the concentration is further increased to 10 mg/ml, there seems to be no dependence of $Z$ on $N_{CL}$.

At the first glance, it is a bit confusing that the PCL-PEO particles obey quite well the scaling relations that were predicted for WSL or SSL, respectively, since the PCL-PEO polymer belongs to the class of amphiphile polymers with large $\chi_{A\text{-}B}$ and $\chi_{A\text{-}Solvent}$. Actually, we were surprised that the particle sizes scaled according to a scaling law at all because the particles are in a highly nonequilibrium state in water so that their dimensions should mainly depend on how they were prepared. Nevertheless, we do believe that the particles preserved their scaling from the initial solvent, where they are in equilibrium and probably close to WSL or SSL. That would mean that the preparation protocol is based on the quenching mechanism, *i.e.*, the initial equilibrated aggregates freeze during fast addition of the polymer solution into water and thus the aggregation numbers do not change. However, because (i) the scaling exponents $\kappa$ and $\mu$ increase with the concentration, (ii) the correlation coefficient for the dependence of $Z$ on $N_{CL}$ becomes the lower the higher is the concentration of the polymer in the initial solution and (iii) there is no trend for the dependence of $Z$ on $N_{CL}$ visible at the highest concentration at all, we assume that the particles are not formed by the pure quenching only, but rather by the quenching mechanism accompanied by the additional particle aggregation during the fast addition of the polymer solution into water. While the aggregation does not play a significant role at low concentrations, resulting in forming of the particles by almost pure quenching, at higher concentrations it is so large that the particle dimensions are practically controlled by the additional aggregation only.

We should not be confused by a relatively good correlation between $R_H$ and $N$ according to $R_H \approx N^{\mu}$ for the whole concentration regime (plot for the $w$ = 10 mg/ml not shown) since $R_H$ considerably changes during the addition of the initial solution into water

due to the collapse of the whole nanoparticle and thus this dependence is not so significant as that of $Z$ on $N_{CL}$.

The fact that the scaling relations valid for micelles control the vesicle sizes at low concentrations indicates that the vesicles probably have only a small cavity in their centre and that they are different from phospholipid vesicles or from those obtained by Eisenberg,[55] whose only parameter that scales is the thickness of the vesicle wall while other parameters such as $R_H$ or $M_w$ exhibit usually broad distributions.

## 6.3. Influence of THF on PCL-PEO Nanoparticles and a Fluorophore Incorporated Inside the PCL Domain

We saw in the previous section how the particle-sizes can be tuned by the change in the composition of the initial THF/water mixture. Now our purpose is to find how tetrahydrofuran influences the nanoparticles once they have been formed. Since our group is interested in fluorescence as much as in light scattering, we solubilized in addition into the PCL domain a hydrophobic fluorescent probe and hoped that by means of various fluorescent techniques we would be able to follow (1) changes in hydration of PCL domain caused by its swelling due to addition of THF into water containing nanoparticles and/or (2) release of fluorescent probes from the PCL domain due to increased solubility of hydrophobic probes in an organic solvent. The latter phenomenon might demonstrate the sensitivity of an incorporated drug poorly soluble in water to a change in external conditions.

### 6.3.1. Changes in Particle Sizes Monitored by Light Scattering

Before applying fluorescence to monitor changes in the system PCL-PEO nanoparticles + a fluorophore, we followed the development of $R_H$ and $M_w$ with the increasing content of THF in the system by light scattering. We prepared a set of samples containing nanoparticles that differed in the content of THF and in the concentration of nanoparticles; the latter difference necessary for extrapolation to the zero concentration in LS. THF was added under vigorous stirring into pure aqueous solutions containing nanoparticles that were prepared from 90 vol.% THF. The samples were let to equilibrate and measured the next day.

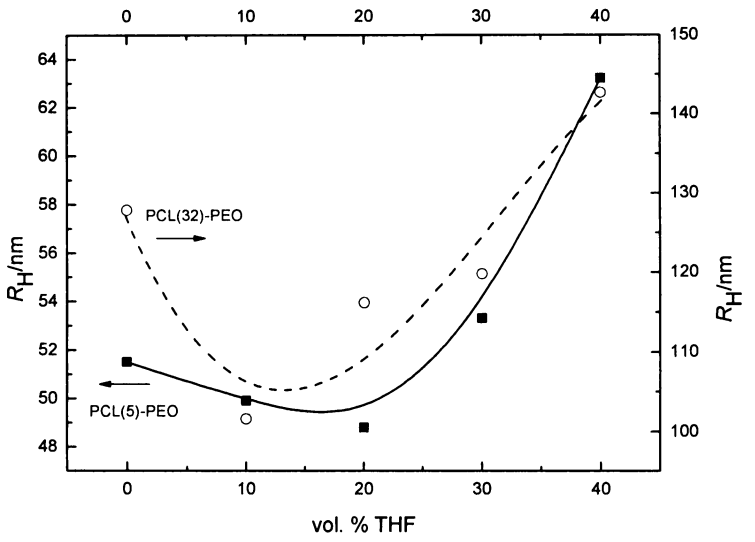


**Fig. 6.11.** Hydrodynamic radii, $R_H$, for PCL(5)-PEO and PCL(32)-PEO nanoparticles as a function of the content of THF in water. The particles were prepared from 90 vol.% THF, where the concentration of the polymer was 10 mg/ml. Similar data were obtained for PCL(13)-PEO and are thus not shown..

As expected, the nanoparticles are sensitive to the presence of THF (see Fig.6.11). Since the weight averaged molar mass of vesicles remains constant during addition of THF (data not shown here), the changes in $R_H$ can be ascribed to swelling or shrinking of the particles and not to aggregation caused by the presence of THF. The first addition of THF leads to the collapse of the PEO domain, for PEO is badly soluble in THF. On the other hand, the PCL domain swells as the content of THF increases in the solution because the solubility of the PCL block is higher in THF than in pure water. The competition of both phenomena results in the observed dependence of $R_H$ on the THF/water ratio.

### 6.3.2. PRODAN and LAURDAN in Water Containing Nanoparticles

For all the following fluorescence measurements, we decided to use fluorescent probes PRODAN and LAURDAN, which have the same chromophore, and thus the same spectroscopic properties, but their acyl chain differs considerably in length. In addition to that, they suit for fluorescence relaxation measurements, which can reveal further worth information on the system studied. Because of relatively high hydrophobicity of both compounds, we supposed that the probes will preferentially sorb into the PCL domain and thus enabling us to monitor its swelling. A very slow decay of correlation functions for PRODAN and LAURDAN, $C(t)$, really confirms that the probes were incorporated into the

hydrophobic domain quite well (see Fig. 6.12). Mean correlation times reaching up to 5 or even 6 ns are typical for a slow relaxation process, which usually occurs in a viscous nonaqueous environment. Almost all water molecules that are present inside the hydrophobic PCL domain are bound to the polymer so that they cannot reorient after the abrupt change of the dipole moment as fast as if they were free. The minimization of the energy (as the development of $C(t)$ with time) is thus mainly controlled by the slow reorientation of the polymer chains. A slightly higher mean correlation time for LAURDAN, $\tau > 5.69$ ns, than for PRODAN, $\tau > 5.35$ ns, suggests that LAURDAN is incorporated in average closer to the centre of the hydrophobic domain than PRODAN, although, as one can see from the difference in the mean times, the difference in positions is probably only small.

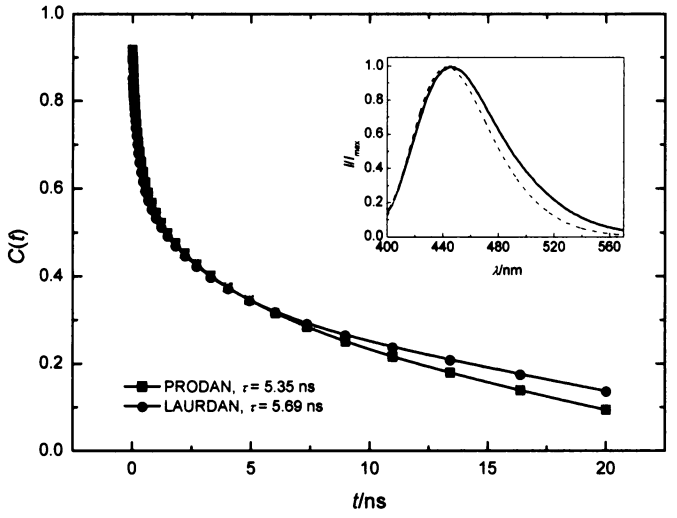


**Fig. 6.12.** Correlation function, $C(t)$, for PRODAN and LAURDAN solubilized into PCL(5)-PEO nanoparticles in aqueous solution. Insert: Normalised steady-state fluorescence spectra for PRODAN (black line) and LAURDAN (red line) solubilized into PCL(5)-PEO particles in water. The concentration of the probes in water was 2.6 μM and that of the polymer in water 0.62 mg/ml. The nanoparticles were prepared from 90 vol.% THF with the concentration of the polymer in the initial solvent $w_i$ = 5 mg/ml.

The observed dependence of the full width at half maximum, FWHM, on the time after excitation (see Fig. 6.13) supports our assumption about the localization of the probes. In the case of LAURDAN, we observe a sharp increase in the FWHM, which is followed by a slow continuous decrease. It corresponds to the relaxation process that is so slow that the lifetime of the excited state of LAURDAN is not long enough to allow us to catch the whole decrease in FWHM and thus the whole relaxation process. This is the reason why we used the sign '>' when expressing the true value of $\tau_R$. The development of the FWHM of

PRODAN exhibits additionally the second increase at longer times. It might indicate that PRODAN is localized in different environments of the hydrophobic domain.

That PRODAN is distributed over a broader range of different microdomains than LAURDAN, is already visible from steady-state fluorescence spectra (see insert in Fig 6.12). SSFS of PRODAN is a bit broadened and shifted about 2 nm to longer wavelengths with respect to the spectrum of LAURDAN, the latter fact supporting the idea that LAURDAN is closer to the centre of the PCL domain.

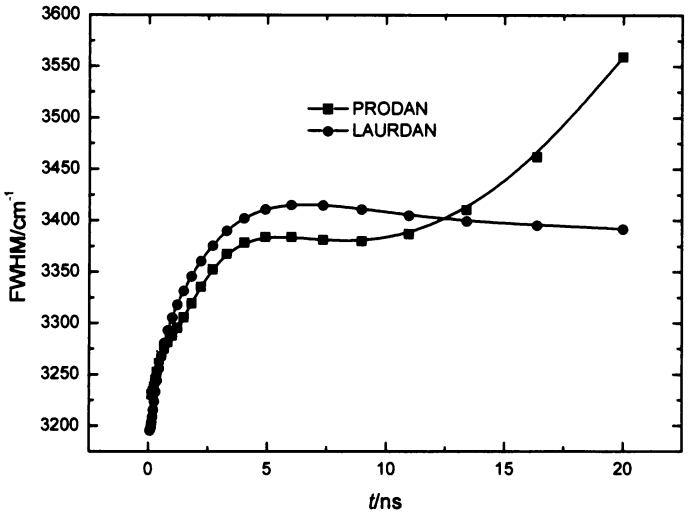


**Fig. 6.13.** Full width at half maximum, FWHM, for PRODAN and LAURDAN solubilized into PCL(5)-PEO nanoparticles in water. The concentrations and the nanoparticles used were the same as in Fig. 6.12.

Based on the facts stated above, we can draw the conclusions that (1) both the probes solubilize quite well into the PCL domain, (2) LAURDAN is better localized inside the PCL domain thanks to its long hydrophobic lauroyl chain and that (3) LAURDAN is in average closer to the centre of the hydrophobic domain, although the difference is not high.

### 6.3.3. Behaviour of PRODAN in THF/Water Mixtures Containing Nanoparticles

Since we wanted to find what happens to PRODAN and the PCL-PEO nanoparticles when THF is added into the aqueous solution, we prepared a set of samples that differed in the content of THF. As model nanoparticles, we chose those formed from the PCL(5)-PEO polymer because the solution containing these particles scatters and absorbs the least light and is consequently clear. The particles were prepared from 90 vol.% THF with the

concentration of the polymer in the initial solvent $w_i$ = 5 mg/ml and the concentration in the final aqueous solution $w_f$ = 1.55 mg/ml. For further details regarding preparation protocol see experimental section, part 5.4.

First of all, we recorded steady-state fluorescence spectra for PRODAN in pure THF/water mixtures (see insert in Fig. 6.14), which served us as reference spectra for mixtures containing nanoparticles. The intensity of SSF spectra significantly increases as the mixture contains more and more THF and, simultaneously, the spectra move to shorter wavelengths. The increase in intensity relates probably to limited solubility of PRODAN in water and its better solubility in THF/water mixtures. Recently, it was even shown that PRODAN aggregates in pure water.[19] The shift of the spectra is, of course, caused by large polarity drop after addition of THF (consider that $\varepsilon$(water) = 80.37 and $\varepsilon$(THF) = 7.58 at 298.15 K).

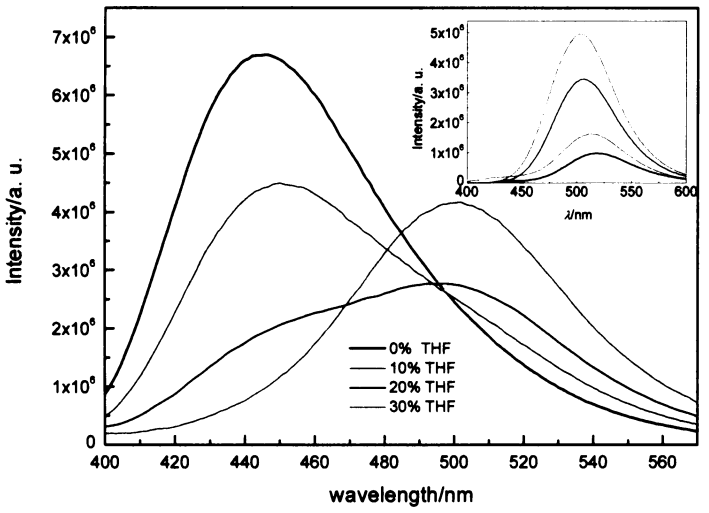


**Fig. 6.14.** Steady-state emission spectra for PRODAN in the system PCL(5)-PEO nanoparticles + THF/water mixture with varying THF/water ratio. Insert: Steady-state emission spectra for PRODAN dissolved in THF/water mixtures. The concentrations are to be found either in the proceeding text or in Fig. 6.12.

Fig. 6.14 shows how the steady-state emission spectra develop with the addition of THF into the polymeric aqueous solution. Mainly the spectrum for 20 vol.% THF/water polymeric solution, which is obviously composed from at least two populations of PRODAN residing in different environments, indicates that the change of spectra is caused by the release of PRODAN from the hydrophobic PCL domain into the bulk solution. After addition of THF, PRODAN has no more so high tendency to hide from the bulk aqueous solution in the PCL hydrophobic domain because THF dissolves PRODAN due to its very low polarity

quite well. PRODAN escapes from the PCL domain so fast that the positions of maxima of the spectra for PRODAN in pure THF/water mixtures and in the mixtures containing particles (compare Fig. 6.14 and insert in Fig. 6.14) coincide almost perfectly already in 30 vol.% THF, meaning that almost all PRODAN have already been released into the bulk solution and that only a minority of PRODAN still resides inside the PCL domain. In order to get a closer look on the release of PRODAN from PCL-PEO particles, we tried to decompose the spectra for 20 and 10 vol.% THF and to estimate at this way at least roughly the populations of PRODAN inside and outside the PCL domain.

#### *6.3.3.1. Spectra Decomposition for 20 vol.% THF/Water Particle Mixture*

At first we began with the decomposition of the steady-state emission spectrum for PRODAN in 20 vol.% THF/water particle mixture because this spectrum consists of two at first sight fairly well developed peaks, whose decomposition should not be, as we hoped, difficult. We assumed that the spectrum is composed from two pure subspectra, the first one belonging to the population of PRODAN residing inside the PCL domain and the other one belonging to PRODAN that emits from the bulk solution. We consequently fitted the emission spectrum in the wavenumber domain by the sum of two log-normal functions, which would have meant to optimize eight different parameters (four for each log-normal function) if we had not managed to reduce the number of parameters to five by recording the emission spectrum of PRODAN in 20 vol.% THF without nanoparticles. It means we optimised only the height for the subspectrum that belongs to PRODAN in the bulk solution and all four parameters, which fully define a log-normal function, for the other subspectrum. Further reduction of the parameters that are to be optimized was unfortunately impossible, because to do so, we would have needed pure subspectrum for PRODAN emitting solely from the PCL domain. Of course, we could have taken the spectrum for PRODAN solubilized into nanoparticles dissolved in water as the second pure subspectrum, since in this case, approximately all the probe molecules are inside the PCL domain (see the proceeding section) and, simultaneously, the fluorescence signal for PRODAN in water is negligible (see insert in Fig. 6.14). However, this further parameter reduction yielded, as we expected, unsatisfying fit mainly because of the wavelength shift between the spectrum for PRODAN in aqueous particle solution (black spectrum in Fig. 6.14) and the virtual spectrum for PRODAN emitting purely from the PCL domain of the PCL-PEO nanoparticles dissolved in

20 vol.% THF (see also the section devoted to LAURDAN and especially Fig. 6.21); the shift caused by the swelling of the PCL domain and consequently by the polarity change inside it.

By fitting of the emission spectrum, we endeavoured to obtain the best fit mainly at both the blue and red edge of the spectrum, *i.e.*, in the region where the first subspectrum is the least influenced by the other and *vice versa*. From Fig. 6.15 we can see that the above described decomposition method yielded very good fit for the whole wavelength range. The decomposed subspectra are then depicted in Fig. 6.16. The blue spectrum belonging to PRODAN still residing inside the PCL domain is blue shifted and its intensity is considerably amplified in comparison to the red spectrum that comes from the emission of PRODAN in the bulk solution because the PCL domain is less polar and more viscous than the bulk solution and because PRODAN has a higher lifetime of the excited state in the PCL domain than outside. The decomposed subspectra are narrow and the fit quite good, which suggests that the decomposition to two subspectra is in this case correct. Since the decomposition may provide ambiguous results we tried to estimate the size of the population of PRODAN inside and outside the PCL domain by as many methods as possible.

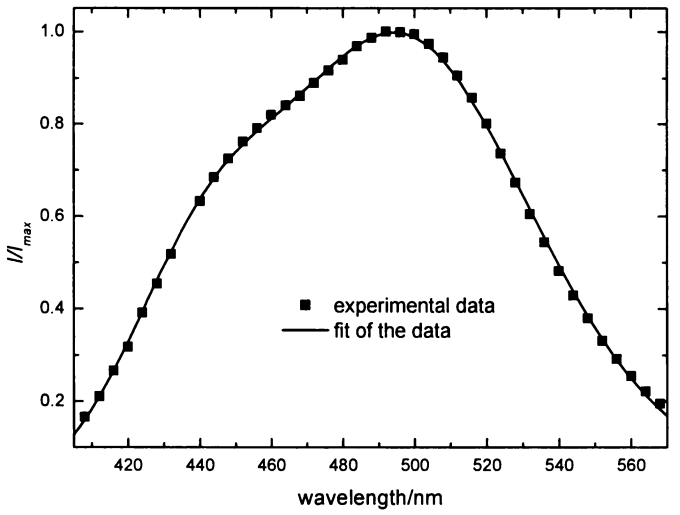


**Fig. 6.15.** Fit of the emission spectrum obtained during the decomposition procedure for PRODAN in 20 vol. % THF/water solution containing PCL(5)-PEO nanoparticles. The concentrations are listed in Fig. 6.12.

1. The first one consists in comparing the peak-height of the decomposed subspectrum belonging to PRODAN that has been released from the PCL domain (the red line in Fig. 6.16) with the peak-height of the steady-state spectrum for PRODAN dissolved in 20 vol.% THF without PCL-PEO particles in the same amount as when dissolved in 20 vol.% THF/water solution containing nanoparticles. The comparison of these

spectra revealed that 66 % of the whole population of PRODAN is in 20 vol.% THF already in the bulk solution and that only 34 % of PRODAN remains still inside the PCL-PEO nanoparticles.

2. On the other hand, one can compare the maximum intensity of the second subspectrum that belongs to PRODAN still residing inside the PCL domain with the maximum intensity of the steady-state spectrum for PRODAN that resides solely in the hydrophobic domain and not in the bulk solution as well. Since this spectrum is poorly accessible for 20 vol.% THF, we replaced this spectrum by the steady-state spectrum for PRODAN incorporated inside the PCL-PEO particles in pure water, where almost all PRODAN resides in the hydrophobic domain (see section 6.3.2). This replacement does not lead to any inaccuracy or inconvenience as suggested by the emission spectra for LAURDAN (see section 6.3.4 and Fig. 6.21), whose peak-height does practically not change when moving from pure water to 20 vol.% THF/water mixture. It means that neither the emission of PRODAN nor that of LAURDAN (consider that both fluorophores have the same chromophore) is considerably influenced by the addition of THF up to 20 vol.% and consequently by the swelling of the PCL domain. This method yielded that 71% of PRODAN is already in the bulk solution when the content of THF reaches 20 vol.%.

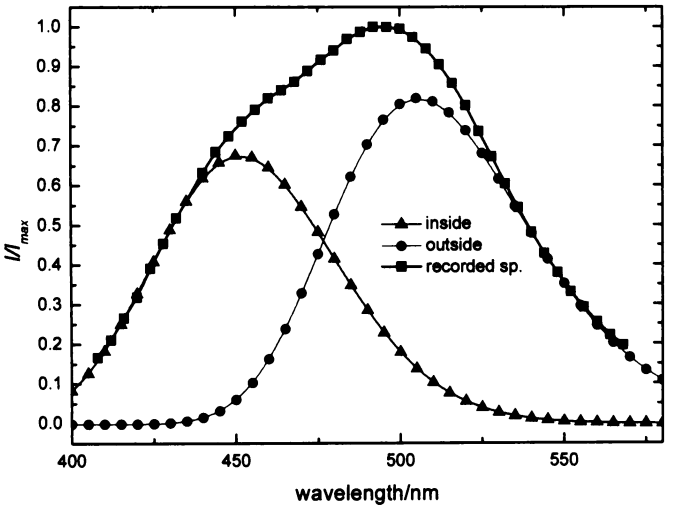


**Fig. 6.16.** Spectra decomposition for PRODAN dissolved in 20 vol.% THF containing PCL(5)-PEO nanoparticles.

3. The partition of PRODAN between the hydrophobic domain and the bulk solution can be estimated not only by the steady-state emission spectra but also by the time-

resolved fluorescence spectra (see Fig. 6.17). For this purpose, the first recorded TRES after excitation is the most convenient, since PRODAN that is still inside the PCL domain has not started to relax yet, so that it emits at the blue edge of the spectrum, while the relaxation of PRODAN that is in the bulk solution is so fast that this population of PRODAN emits all light from the relaxed state at the red edge of the spectrum. Both peaks are thus well separated from each other, which makes the estimation easier. By comparing the peak-heights of the first recorded TRES (see Fig. 6.17, green line), we determined the size of the population of PRODAN residing outside the domain to 71 % after having corrected the peak-heights to the fact that PRODAN emits in different environments with different intensities.

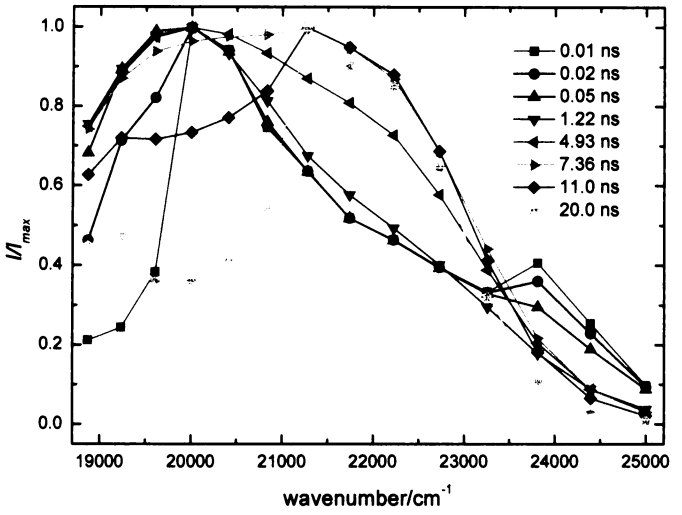


**Fig. 6.17.** Time-resolved fluorescence spectra for PRODAN dissolved in 20 vol.% THF containing PCL(5)-PEO nanoparticles.

As we can see, three different, although not completely mutually independent, methods, by means of which we tried to estimate the extent of release of PRODAN from the hydrophobic PCL domain after the change of external conditions, yield almost the same results. In addition to that, both decomposed subspectra are narrow and the fit of the emission spectrum is good enough so that it is not necessary to involve a third subspectrum into the decomposition procedure. Hence, we can conclude that relatively small change in external conditions, *i.e.*, the addition of THF up to 20 vol.%, brings about burst release of PRODAN into the bulk solution. Only a minority of PRODAN reaching 30 % of the whole population that was incorporated well in the very centre of the PCL domain remains inside the domain.

Nevertheless, even this minority of PRODAN is released from the hydrophobic centre when further 10 vol.% of THF is added into the solution.

Before coming over to the spectra decomposition for 10 vol.% THF particle-PRODAN solution, it is worth to comment, thanks to its unusualness, at least a bit the development of TRES with time in Fig. 6.17. The diversity is a result of the presence of two emitting populations of PRODAN residing in completely different environments. The intensity drop of the peak near 24000 $cm^{-1}$, which belongs to PRODAN residing inside the PCL domain, is caused by the relaxation process occurring on the nanosecond timescale. This peak moves to lower frequencies and becomes the most intensive at the end of the measurement. The second well-developed peak near 20000 $cm^{-1}$ belongs to PRODAN emitting from the bulk solution. This peak does not move during the course of the measurement because the relaxation process is so fast that it is beyond the resolution of our equipment. However, the peak intensity drastically decreases with time, because the lifetime of the excited state of PRODAN in the bulk solution is much lower than that for PRODAN incorporated into the hydrophobic domain. Another consequence of the short lifetime of PRODAN in the bulk solution compared to the other population of PRODAN is relatively high intensity of the blue decomposed subspectrum in Fig. 6.16, which almost reaches the intensity of the red subspectrum, although only about 30 % of the whole population of PRODAN emits at the blue edge of the spectrum.

#### *6.3.3.2. Spectra Decomposition for 10 vol.% THF/Water Particle Mixture*

To decompose the steady-state emission spectrum would not have been, in this particular case, as convenient as for PRODAN in 20 vol.% THF/water particle mixture because this spectrum misses at least a hint of the second maximum belonging to PRODAN in the bulk solution (see the red line in Fig. 6.14) due to weak fluorescence of PRODAN in 10 vol.% THF (see insert in Fig. 6.14) and due to lower release of the probe from the PCL domain. Such decomposition could be tricky with respect to the danger of fitting noise and, as we found, it really gained unsatisfying fit. On the contrary, since time-resolved fluorescence spectra are not as much influenced by the great difference between lifetimes of PRODAN inside and outside particles as SSFS, the first TRES possesses two well-developed maxima (see Fig. 6.18). That is why we concentrated on the decomposition of the time-resolved fluorescence spectrum instead of steady-state one.

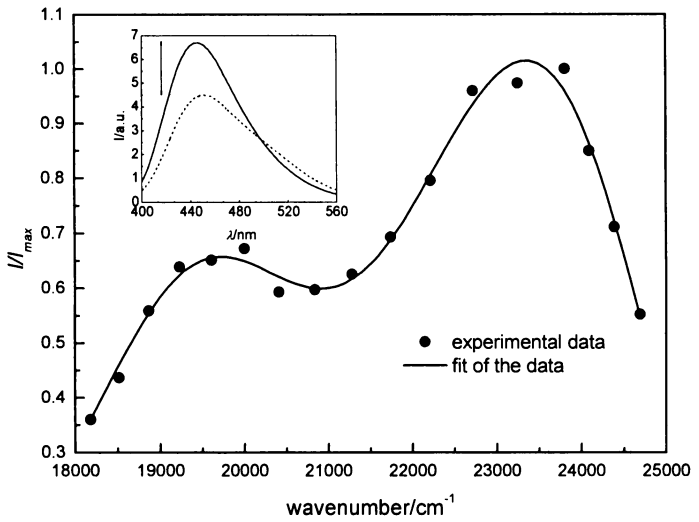


**Fig. 6.18.** Fit of the first recorded time-resolved fluorescence spectrum for PRODAN in 10 vol.% THF/water particle mixture based on the in text described decomposition method. Insert: Drop of the intensity at maximum when going from pure water to 10 vol.% THF/water particle mixture corresponding to the partial release of PRODAN into the bulk solution. For concentrations see Fig. 6.12.

The decomposition method consisted, as in the previous case, in optimising 'only' five different parameters for the sum of two log-normal functions, for the recorded pure TRES for PRODAN in 10 vol.% THF without nanoparticles helped us to reduce the three remaining parameters. After having obtained the optimized parameters, we reconstructed both time-resolved subspectra (see Fig. 6.19) and estimated the extent of the PRODAN release from the PCL domain by comparing the peak-heights of both decomposed subspectra between each other. Once again, before doing that, we had to correct the fluorescence intensities by means of the TRES for PRODAN dissolved in pure 10 vol.% THF and the PRODAN TRES recorded in pure water with nanoparticles. We found at this way that 35 % of the whole amount of PRODAN was released into the bulk solution after addition of 10 vol.% of THF. This result is in the full agreement with that what one would expect, since the addition of half amount of THF (10 vol.% instead of 20 vol.%) led to the two-fold decrease of the PRODAN release outside (from 71 % to 35 %).

To be sure the decomposition did not provide misleading data, we determined the amount of released PRODAN by the intensity drop of the SSFS for PRODAN in 10 vol.% THF particle solution with respect to the SSFS for PRODAN in pure water containing particles, in which approximately all the probe molecules are incorporated in the PCL domain, as well (see insert in Fig. 6.18). As in the previous case, taking into account the

experiments carried out with LAURDAN, we do believe that PRODAN emits with equal intensity from inside the particles independently on whether the nanoparticles are dissolved in pure water or in 10 vol.% THF. Under this assumption, the intensity drop about 32 % gives the direct evidence that ca 32 % of PRODAN is already in the bulk solution.

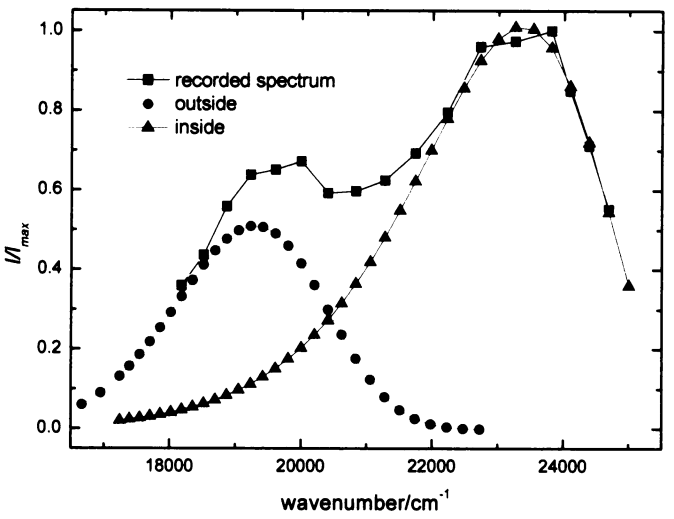


**Fig. 6.19.** Decomposition of the experimental spectrum with two well-developed maxima belonging to PRODAN dissolved in 10 vol.% THF/water PCL(5)-PEO particle mixture (black line) to two subspectra.

Further information on the behaviour of PRODAN in the 10 vol.% THF particle solution can provide us the development of the maximum of the blue subspectrum in Fig. 6.19 with time, *i.e.*, the correlation function, $C(t)$. In order to imagine which changes occurred in the system after THF was added, we compared the correlation function for the blue subspectrum with $C(t)$ for PRODAN incorporated into the particles in pure water (see Fig. 6.20). Relatively high difference of the development of $C(t)$ and relatively high drop of the mean correlation time from 5.35 to 1.85 ns indicates that substantial changes must have occurred in the system. They may be ascribed either to the swelling of the PCL domain or to the relocation of the rest of the PRODAN population that remained inside the particles or to both phenomena. Since the experiments carried out with LAURDAN have shown that the mean correlation time can change only about 1 ns as the consequence of the swelling of the PCL domain brought about by the addition of THF up to 10 vol.% (see the following section), the change of $\tau$ about at least 2.5 ns ( = 5.35 ns – 1.85 ns – 1.00 ns) has been caused by the relocation of the rest of PRODAN to a less viscous environment, *i.e.*, closer to the bulk solution. A more detailed look at the blue subspectrum in Fig. 6.19 reveals further its

long shoulder in the direction to lower frequencies, which supports the idea, together with the broadening of the blue subspectrum with respect to the TRES for PRODAN incorporated into the particles dissolved in pure water (this spectrum is not shown here), that indispensable part of PRODAN was relocated closer to the bulk solution, although, as suggested by a small shift of the SSFS to longer wavelengths (see insert in Fig. 6.18), a certain amount of PRODAN remained probably near the centre of the hydrophobic domain. One could even speculate that PRODAN that is near the very centre of the PCL domain stands up to the next addition of THF and remains thus still inside the particles while the rest of PRODAN is definitively washed out.

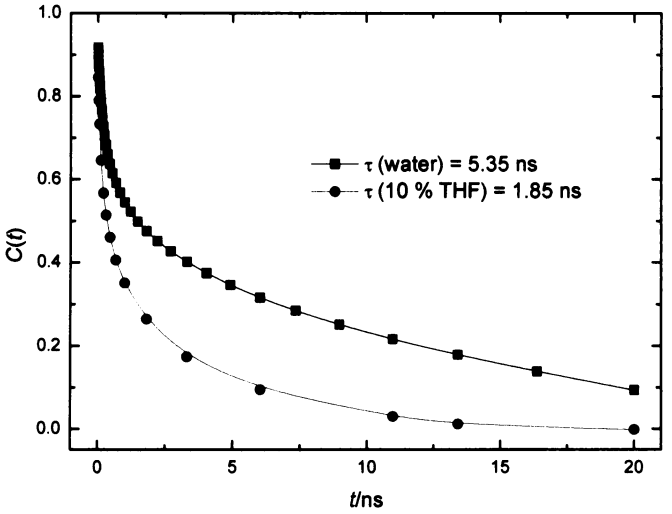


**Fig. 6.20.** Correlation functions for PRODAN dissolved in pure water or in 10 vol.% THF/water mixture, respectively, together with PCL(5)-PEO nanoparticles. The blue curve describes the development of the maximum of the blue subspectrum in Fig. 6.19. The correlation function is thus related solely to PRODAN that resides inside the particles.

### 6.3.4. Behaviour of LAURDAN in THF/Water Mixtures Containing Nanoparticles

Because a relatively small molecule of PRODAN has a high tendency to be released from the nanoparticles after addition of THF, we tried to find whether a prolongation of the acyl chain of PRODAN, in our case the substitution of PRODAN by LAURDAN, will help to hinder, at least in part, the large release of the probe from the PCL domain.

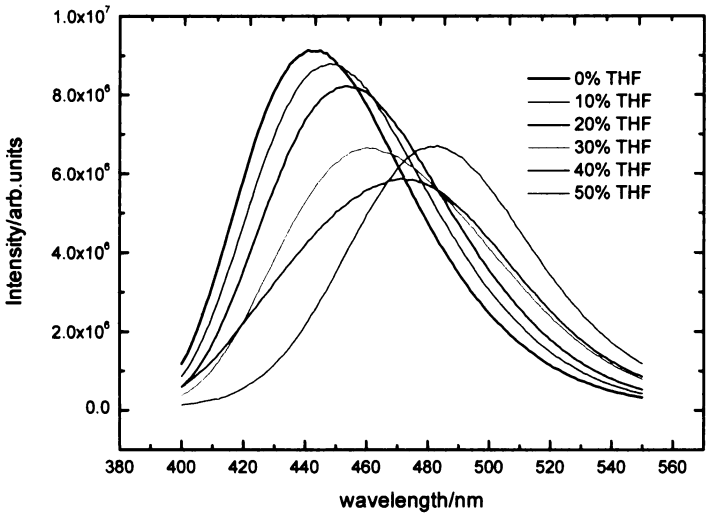


**Fig. 6.21.** The development of steady-state fluorescence spectra of LAURDAN as THF is added into the PCL(5)-PEO particle solution. The nanoparticles were prepared from 90 vol.% THF with the concentration of the polymer in the initial solvent $w_i$ = 5 mg/ml. The concentration of the probes in water was 2.6 μM and that of the polymer in water 0.62 mg/ml. This is we worked in the same concentration regime and with the same nanoparticles as in the case of PRODAN.

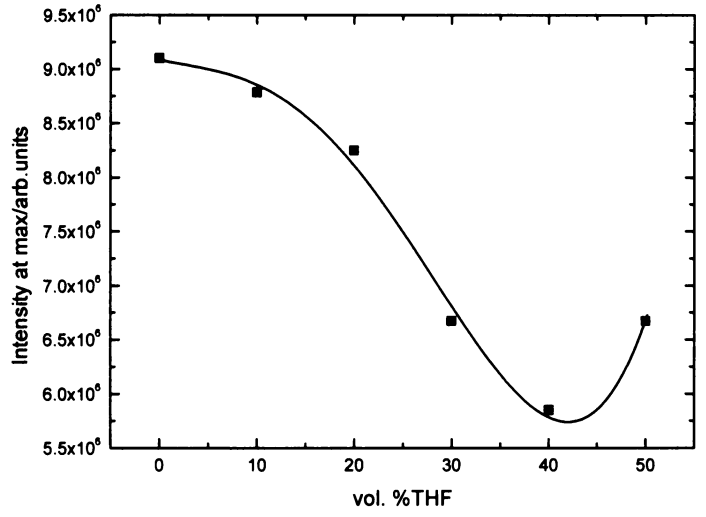


**Fig. 6.22.** Intensity at maximum of the steady-state fluorescence spectra in Fig. 6.21 as a function of the content of THF in the particle solution.

The steady-state emission spectra really exhibit smaller decrease of the intensity at maximum (see Fig. 6.21 and Fig. 6.22) in comparison to SSFS for PRODAN (see Fig. 6.14),

indicating that LAURDAN is able to remain inside the PCL domain substantially longer, although even LAURDAN is released finally as well. Up to 20 vol. % of THF in THF/water mixture, the maximum intensity changes only a little, mainly as the consequence of swelling and of a very small release of the probe, the latter fact having the two following reasons. Firstly, the experiments carried out with LAURDAN dissolved in the particle aqueous solution have shown that the probe incorporates into the very centre of the hydrophobic domain, from which, one may assume, it is not so easy to get out. Secondly, LAURDAN has a very long acyl chain that considerably constrains free movement of the probe inside the domain. The fact that the intensity is up to 20 vol. % almost constant (after excluding the intensity drop brought about by the release) enabled us to replace the maximum intensity of the SSFS for PRODAN in 10 and 20 vol. % THF by the SSFS in pure water (see the decomposition in section 6.3.3).

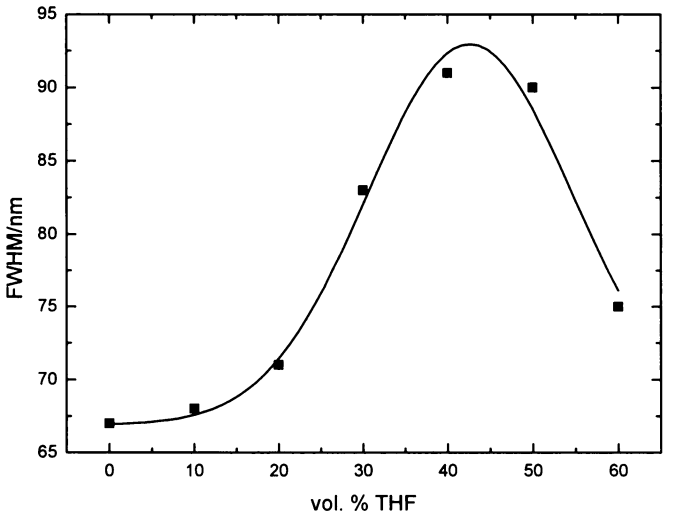


**Fig. 6.23.** Full width at half maximum, FWHM, of the steady-state emission spectra in Fig. 6.21 as a function of the content of THF in the particle mixture.

However, the more THF is added, the more the PCL domain swells and the more soluble becomes the bulk solution for LAURDAN. These circumstances lead to enhanced sequential release of the probe beginning at the content of THF near 20 vol. %. The release together with the swelling causes a sharp decrease of the intensity in the region between 20 and 40 vol. % THF (see Fig. 6.22). Because LAURDAN exhibits better solubility in THF than in water and the consequently stronger fluorescence in the former solvent, we do finally observe an increase of the intensity.

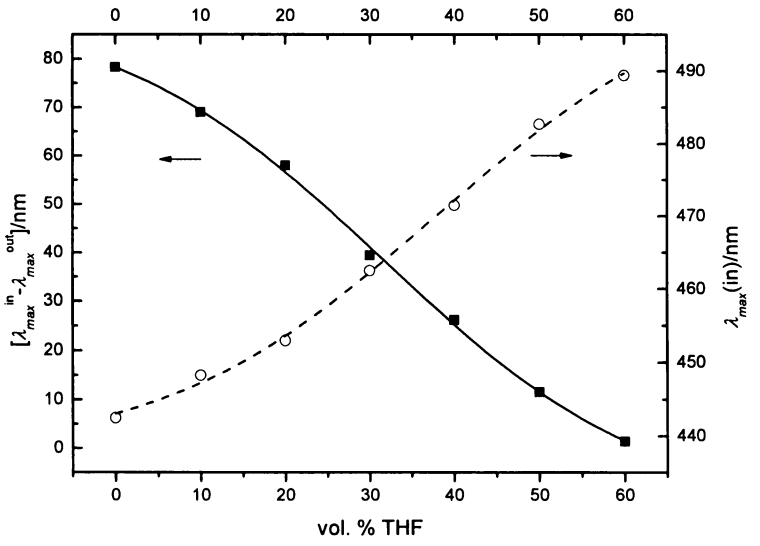


**Fig. 6.24.** Dashed line: Positions of the peak maximum of steady-state fluorescence spectra in Fig. 6.21 as a function of the content of THF in the particle mixture. Solid line: Difference of peak maxima of the SSFS for LAURDAN dissolved in the particle mixture and the SSFS for PRODAN dissolved in pure THF/water mixtures without nanoparticles as a function of the content of THF in the solutions. We replaced PRODAN by LAURDAN due to better solubility of the former in the solutions rich in water.

Closer insight into the behaviour of LAURDAN after THF addition can provide us development of the full width at half maximum, FWHM, of the SSFS in Fig. 6.21, for FWHM reaches the higher values the broader is the distribution of different environments of a probe. Up to 10 or 20 vol. % THF, the FWHM increases only negligibly (see Fig. 6.23). Nevertheless, even this low change gives evidence that a small part of the whole population of LAURDAN was relocated to less polar and/or less viscous microenvironment within the particles. The probe must have been relocated mainly within the nanoparticles and was probably only in a negligible amount (especially after first addition of THF) released into the bulk solution because the intensity drop of SSFS after THF addition up to 20 vol. % is only small and a very weak fluorescence of LAURDAN from the solutions rich in water and without nanoparticles would have been entirely insufficient to significantly broaden the SSFS for LAURDAN in 10 or 20 vol. % THF, respectively. However, the fluorescence increases with the increasing content of THF in water (similar as in the case of PRODAN), and so we can later observe emission both from inside and outside the particles. The distribution of different localizations is the broadest in about 40 vol. % THF and starts to decrease from this point as more and more LAURDAN is found in the bulk solution.

As LAURDAN moves towards the bulk solution and as more solvent penetrates into the particles during their swelling, the probe relaxes in a larger extent, and the SSFS shift to longer wavelengths (see Fig. 6.24, dashed line). Most substantial changes occur near 30 vol. % THF, where the sigmoidal curve has its inflection point. How much LAURDAN has already been released from inside the particles can also be determined by plotting the difference of the peak positions of the SSFS in Fig. 6.21 and the SSFS for LAURDAN in pure solvents without nanoparticles (for the plot see Fig. 6.24, solid line). Due to experimental difficulties to dissolve LAURDAN in solvents rich in water or even in pure water, we replaced the LAURDAN SSFS by PRODAN SSFS when determining the peak-position of spectra recorded from pure solvents. The difference of the peak positions is the highest before the first addition of THF because all LAURDAN is in this case inside the particles. On the other hand, both spectra are almost identical in 60 vol. % THF, no matter whether the solution contains the polymer or not, and the difference is negligible At this place we should note that the nanoparticles are so much swollen in 60 vol. % THF that it makes no more sense to distinguish between 'inside and outside the particles'

At the beginning of the section devoted to fluorescence, we mentioned our purpose to observe swelling of the PCL domain by means of fluorescence techniques. Such an observation, however, is complicated by the strong tendency of both probes to redistribute after addition of THF. That is we are not able to say exactly which part of the overall change can be ascribed to the swelling and which one to the release. Nevertheless, a relatively slow release of LAURDAN from the PCL domain after first additions of THF enables at least to judge about the extent of swelling. As seen from Fig. 6.24, dashed line, and Fig. 6.23, the relative shift of $\lambda_{max}$ between the two SSFS is 12.6 % when going from pure water to 10 vol. % THF while the FWHM increases only about 3.1 %, which may indicate that the change of spectra after first addition of THF mainly arises from swelling of the PCL domain (the influence of redistribution is not as important as the change of polarity and/or viscosity). Let us consider also the large change in the FWHM of the PRODAN SSFS equal to 17.8 nm and the small change in the FWHM of LAURDAN SSFS equal to only 1 nm. Already the second addition of THF leads to the relative change of $\lambda_{max}$ of about 22.4% but a significantly larger increase of the FWHM about 15.8 %. Therefore, the development of fluorescence spectra is the more controlled by the release the more THF is added. However, as illustrated above, we can assume that the changes up to 10 vol. % THF are from great part caused by the swelling.

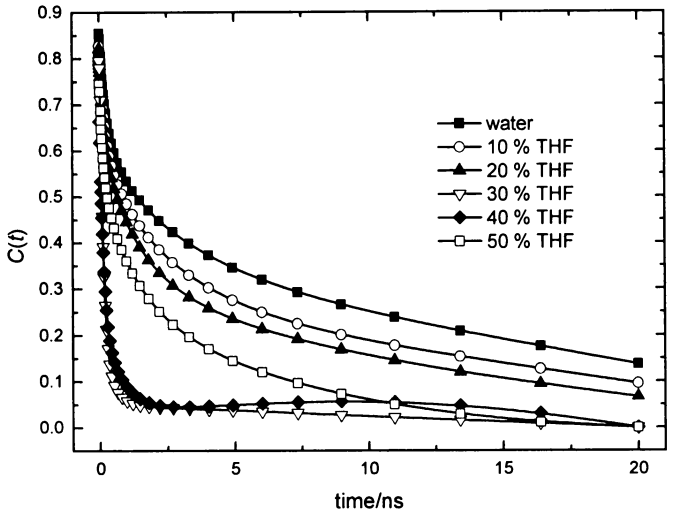


**Fig. 6.25.** Correlation functions, $C(t)$, for LAURDAN dissolved in PCL(5)-PEO particle mixtures differing in the THF/water ratio.

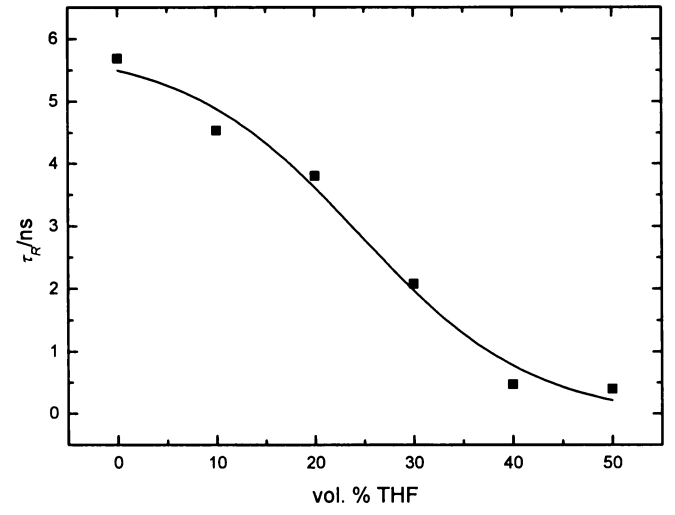


**Fig. 6.26.** Mean correlation time, $\tau_R$, as a function of the content of THF in the THF/water PCL(5)-PEO particle mixtures. The time $\tau_R$ equals the area under correlation curves in Fig. 6.25

Therefore, also the change of the mean correlation time, $\tau_R$, after first addition of THF can be mainly, but not entirely, ascribed to the swelling of the PCL domain (see Figs. 6.25 and 6.26). The mean correlation time decreases then from the initial 5.69 ns to ca 4.55 ns. That is, the first addition of THF brought about a relatively high drop of the viscosity inside the particles, since changes of $\tau_R$ only about 0.1 ns may already give an evidence that substantial changes occurred in the system. The mean correlation time decreases

continuously with further addition of THF as the relaxation becomes faster due to swelling and also due to release, which even prevails over the swelling from 20 vol. % THF onward. The curve has a sigmoidal shape as those in Fig. 6.24, the only difference is that the inflection point is shifted about 6 vol. % THF to the left. That might be caused by a higher sensitivity of $\tau_R$ to the viscosity changes occurring in the system. However, the sensitivity becomes worse as more THF is added, since the relaxation is then so fast that it is beyond the resolution of our equipment (see an almost constant profile of $\tau_R$ between 40 and 50 vol. % THF).

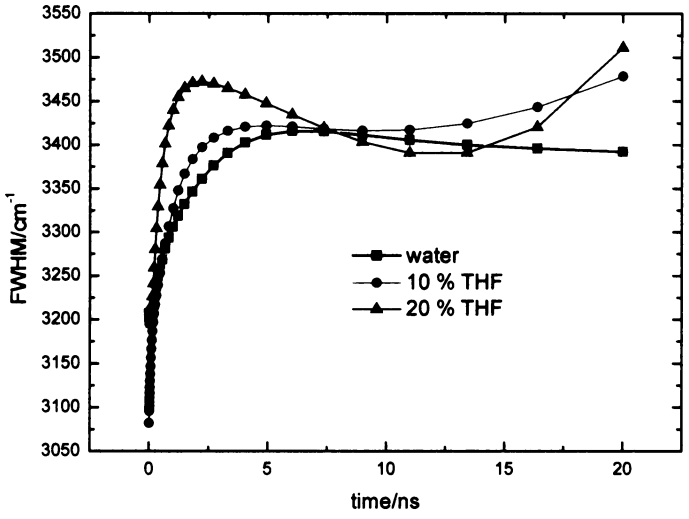


**Fig. 6.27.** Dependence of the full width at half maximum, FWHM, on the time after excitation for LAURDAN dissolved in the PCL(5)-PEO particle THF/water mixtures differing in the content of THF.

The correlation functions, $C(t)$, from which the $\tau_R$ is calculated by integration, are depicted in Fig. 6.25. However, the development of the peak maxima provides us, in this particular case, solely the average information on the whole system because the spectra are very broad due to different localizations of LAURDAN, especially after a substantial amount of THF was added. The peak maximum is thus influenced both by the population of LAURDAN residing still inside and the population of LAURDAN that has been already released.

Just for illustration, we can estimate the rate of relaxation from the dependence of the full width at half maximum, FWHM, of the TRES on time as well (see Fig. 6.27). The initial growth of the FWHM is the higher the more THF the solution contains. The FWHM thus confirms that the relaxation becomes faster as more and more THF is added. But not only that, the final upturn of the curves for 10 and 20 vol. % THF indicates a partial relocation of

LAURDAN. Since we observe a small upturn already for 10 vol. % THF, we must not exclude that relocation has also an influence on the spectral changes after the first addition of THF.

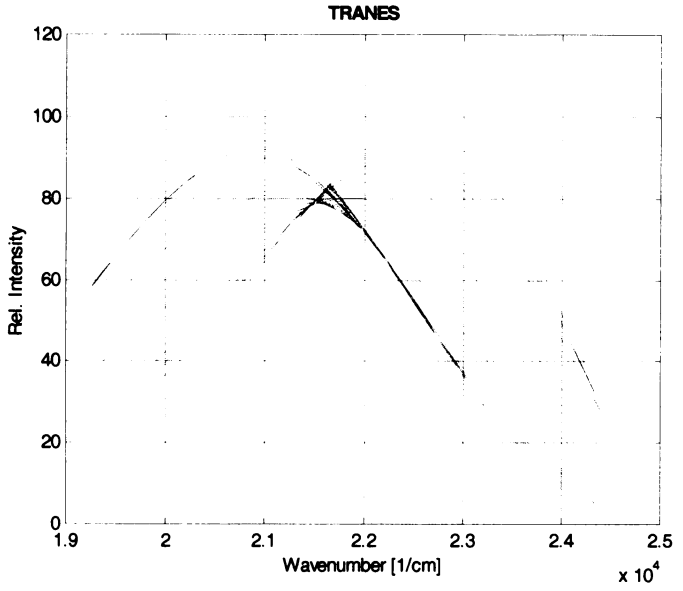


**Fig. 6.28.** Time-resolved area-normalized emission spectra for LAURDAN dissolved in 40 vol. % THF/water PCL(5)-PEO particle mixture. The spectra were recorded in the time span 0–20 ns after excitation. As the relaxation proceeds, the spectra shift to lower frequencies.

Direct evidence of different localizations of LAURDAN can give us time-resolved area normalized emission spectra, TRANES. We present here such a spectrum for 40 vol. % particle THF/water mixture. LAURDAN exhibits sufficient fluorescence from the bulk solution of this composition and some dye molecules remain probably still inside the particles, so that TRANES could, as we hoped, reveal different localizations of the probe. Really, TRANES possess one isoemisive point, suggesting that LAURDAN resides in two completely different microenvironments. The peak positions of TRANES are in agreement with our assumption that one part of LAURDAN resides inside the particles and the other in the bulk solution.

## 7. Conclusions

- All three PCL-PEO polymers differing in the length of the PCL block are quite well soluble in pure tetrahydrofuran. The addition of water up to 10 vol. % improves the solubility of PCL(5)-PEO and PCL(13)-PEO even further while the solubility of PCL(32)-PEO becomes worse due to the long hydrophobic PCL block.
- Direct dialysis of the THF or THF/water polymer solutions against water leads to large polydisperse particles with the size of $10^3$ nm. On the other hand, slow addition of the polymer solutions into water and following dialysis gain well-defined stable nanoparticles, whose dimensions strongly depend on the composition, *i.e.*, on the THF/water ratio of the initial solvents and on the concentration of the polymers in the THF/water mixtures. While relatively monodisperse particles with $R_H$ lower than 110 nm are formed from pure and 90 vol. % THF, further reduction of the THF content in the initial solvents leads to large polydisperse particles. In addition to that, the particles are the smaller the lower is the concentration of the polymers in the initial solvents.
- The dimensions of the particles that were transferred into water correlate with the dimensions of the aggregates that are found in THF/water mixtures. As shown, the final nanoparticles are formed by two competitive processes, *i.e.*, by quenching mechanism and additional aggregation during the addition of the polymer solutions into water. The tendency to aggregate is the more pronounced the more polymer is contained in the initial solvents.
- The nanoparticles that were transferred into water from the initial solvents in which the polymer concentration was sufficiently low follow quite well scaling relations valid for WSL or SSL. We do believe that the nanoparticles preserved their scaling relations from the initial solvents. However, as the polymer concentration in the organic solvents increases, the particles aggregate more and more during addition into water, and the scaling relations cease being valid.
- Vesicles with relatively thick vesicle-wall are formed from all three PCL-PEO polymers. The high wall-thickness is probably the reason why the particles follow quite well the scaling relations for micelles.
- Addition of THF into aqueous particle solution brings about the swelling of the PCL domain and the simultaneous shrinking of the PEO domain.

- Both fluorescent probes PRODAN and LAURDAN incorporate quite well into the hydrophobic PCL domain. Nevertheless, LAURDAN is better localized inside the particles and resides in average closer to the centre of the PCL domain, though the difference is not high.
- PRODAN with a short acyl chain has very low binding affinity to inner parts of the particles after a small amount of THF is added. By the decomposition of SSFS and TRFS we were able to estimate the extent of release of PRODAN from inside the particles for 10 and 20 vol. % THF. The decomposition methods revealed that about 35 or even 70 %, respectively, of PRODAN was released into the bulk solution after THF up to 10 or 20 vol. %, respectively, had been added. This experiment might demonstrate the sensitivity of an incorporated drug to the relatively small change in the external conditions.
- LAURDAN with a long acyl chain is released from inside the PCL domain substantially slower, which enabled us, at least after first two additions of THF up to 20 vol. %, to observe swelling of the PCL domain by means of fluorescence techniques. We assume that for 10 vol. % THF, the drop of the mean correlation time is mainly, but not entirely, caused by the swelling while for 20 vol. % THF, the further drop is brought about by the swelling and substantially also by the release. Further addition of THF results in burst release of the probe, so that it is no more possible to observe swelling by means of LAURDAN. To use fluorescence techniques for observing the swelling of the PCL domain more precisely, we would need a fluorescence tag chemically bound to the PCL-PEO polymer.

## 8. References


1) Gan, Z; Fung, J.T.; Jing, X.; Wung, C.; Kuliche, W.K. *Polymer* **1998**, 40, 1961.
2) Zhao, Y.; Hu, T.; Lv, Z.; Wang, S.; Wu, C. *J. Polym. Sci.* **1999**, 37, 3288.
3) Soo, P.L.; Luo, L.; Maysinger, D.; Eisenberg, A. *Langmuir* **2002**, 18, 9996.
4) Aliabadi, H.M.; Mahmud, A.; Sharifabadi, A.D.; Lavasanifar, A. *J. Controlled Release* **2005**, 104, 301.
5) Ge, H.; Hu, Y.; Cheng, D.; Yuan, Y.; Bi, H.; Yang, C. *J. Pharm. Sci* **2002**, 91, 1463.
6) Aliabadi, H.M.; Brocks, D.R.; Lavasanifar, A. *Biomaterials* **2005**, 26, 7251.
7) Vangeyte, P.; Gautier, S.; Jérôme, R. *Colloids Surf. A: Physicochem. Eng. Aspects* **2004**, 242, 203.
8) Vangeyte, P.; Leyh, B.; Heinrich, M.; Grandjean, J.; Bourgaux, C.; Jérôme, R. *Langmuir* **2004**, 20, 8442.
9) Šachl, R.; Uchman M.; Matějíček, P.; Procházka, K.; Štěpánek, M. *Langmuir* **2007**, 23, 3395.
10) Xu, R.; Winnik, M.A.; Riess, G.; Chu, B.; Croucher, M.D. *Macromolecules* **1991**, 25, 644.
11) Bronstein, L.M.; Chernyshov, D.M.; Timofeeva, G.I., Dubrovina, L.V.; Valetsky, P.M. *Langmuir* **1999**, 15, 6195.
12) Bromberg, L.; Magner, E. *Langmuir* **1999**, 15, 6792.
13) Rapoport, N.; Marin, A.; Luo, Y.; Prestwich, G.D.; Muniruzzaman, M. *J. Pharm. Sci.* **2002**, 91, 157.
14) Yu, B.G.; Okano, T.; Kataoka, K.; Sardari, S.; Kwon, G.S. *J. Controlled Release* **1998**, 56, 285.
15) Lee, J.; Cho, E.C.; Cho, K. *J. Controlled Release* **2004**, 94, 323.
16) Nah, J.W.; Jeong, Y.I.; Cho, C.S.; Kim, S.I.J. *Appl. Polym. Sci.* **2000**, 75, 1115.
17) Vangeyte, P.; Jérôme, R. *J. Polym. Sci., Part A: Polym. Chem.* **2004**, 42, 1132.
18) Liu, J.; Xiao, Y.; Allen, C. *J. Pharm. Sci* **2004**, 93, 132.
19) Moyano, F.; Biasutti, M.A.; Silber, J.J.; Correa, N.M. *J. Phys. Chem.* **2006**, 110, 11838.
20) Parasassi, T.; Krasnowska, E.K.; Bagatolli, L.; Gratton, E. *J. Fluoresc.* **1998**, 8, 365.
21) Viard, M.; Gallay, J.; Vincent, M.; Paternostre, M. *Biophys. J.* **2001**, 80, 347.
22) Jurkiewicz, P.; Olżińska, A.; Langner, M.; Hof, M. *Langmuir* **2006**, 22, 8741.

23) Jurkiewicz, P.; Sýkora, J.; Olžińska, A; Humpolíčková, J.; Hof, M. *J. Fluoresc.* **2005**, 15, 883.

24) Sýkora, J.; Kapusta, P.; Fidler, V.; Hof, M. *Langmuir* **2002**, 18, 571.

25) Humpolíčková, J.; Štěpánek, M.; Procházka, K.; Hof,, M. *J. Phys. Chem. A* **2005**, 109(48), 10803.

26) Weber, G.; Farris, F.J. *Biochemistry* **1979**, 18, 3075.

27) Balter, A.; Nowak, W.; Pawełkiewicz, W.; Kowalczyk, A. *Chem. Phys. Letters* **1988**, 143, 565.

28) Viard, M.; Gallay, J.; Vincent, M., Meyer, O.; Robert, B.; Paternostre, M. *Biophys. J.* **1997**, 73, 2221.

29) Frauchiger, L.; Shirota, H.; Uhrich, K.E.; Castner, E.W. *J. Phys. Chem.B* **2002**, 106, 7463.

30) Kelkar, D.A.; Chattopadhyay, A. *J. Phys. Chem. B* **2004**, 108, 12151.

31) Sýkora, J.; Kapusta, P.; Fidler, V.; Hof, M. *Langmuir* **2002**, 18, 571.

32) Hutterer, Z.; Schneider, F.W.; Sprinz, H.; Hof, M. *Biophys. Chem.* **1996**, 61, 151.

33) Sheynis, T.; Sýkora, B.; Benda, A.; Kolusheva, S.; Hof, M.; Jelínek, R. *Eur. J. Biochem.* **2003**, 270, 4478.

34) Hutterer, R.; Schneider, F.W.; Hermens, W.T.; Wagenvoord, R.; Hof, M. *Biochim. Biophys. Acta* **1998**, 1414, 155.

35) Sýkora, J.; Mudogo, V.; Hutterer, R.; Nepraš, M.; Vaněrka, J.; Kapusta, P.; Fidler, V.; Hof, M. *Langmuir* **2002**, 18, 9276.

36) Sýkora, J.; Jurkiewicz, P.; Epand, R.M.; Kraayenhof, R.; Langner, M.; Hof, M. *Chem. Phys. Lipids* **2005**, 135, 213.

37) Wong, J.E.; Duchscherer, T.M.; Pietraru, G.; Cramb, D.T. *Langmuir* **1999**, 15, 6181.

38) Sengupta, B.; Guharay, J.; Sengupta, P.K. *Spectrochim. Acta Part A* **2000**, 56, 1433.

39) Burchard, W. *Light Scattering. Principles and Development*; Brown, W., Ed.; Clarendon Press: Oxford, 1996.

40) Huglin, M.B. In *Light Scattering from Polymer Solutions*; Huglin, M.B., Ed.; Academic Press: London, 1972.

*41)* Andersson, M.;Wittgren, B.; Wahlund, K.G. *Anal. Chem.***2003**, 75, 4279.

42) Lakowicz, J.R. *Principles of Fluorescence Spectroscopy*; Plenum Press: New York, 1983.

43) Lakowicz, J.R. *Topics in Fluorescence Spectroscopy, Principles*; Plenum Press: New York, 1991.

44) Hof, M. In *Solvent Relaxation in Biomembranes (Applied Fluorescence in Chemistry, Biology and Chemistry)*; Retting, W., Ed.; Springer Verlag: Berlin, 1999; p 439.

45) Hutterer, R.; Parusel, A.B.J.; Hof, M. *J. Fluoresc* **1998**, 8, 389.

46) Horng, M.L.; Gardecki, J.A.; Papazyan, A.; Maroncelli, M. *J. Phys. Chem.* **1995**, 99, 17311.

47) Fee, R.S.; Maroncelli, M. *Chem. Phys.* **1994**, 183, 235.

48) Matějíček, P.; Humpolíčková, J.; Procházka, K.; Tuzar, Z.; Špírková M.; Hof, M.; Webber, S.E. *J. Phys. Chem. B* **2003**, 107, 8232.

49) Štěpánek, M.; Matějíček, P.; Humpolíčková, J.; Procházka, K. *Langmuir* **2005**, 21, 10783.

50) Humpolíčková, J.; Procházka, K.; Hof, M.; Tuzar, Z.; Špírková, M. *Langmuir* **2003**, 19, 4111.

51) In *Polymer Handbook*, 3rd ed.; Brandup, J.; Immergur, E.H., Eds.; Wiley Interscience: New York, 1989.

52) Wu, C.; Woo, K.F.; Luo, X.; Ma, D.-Z. *Macromolecules* **1994**, 27, 6055.

53) Nayak, J.N.; Aralaguppi, M.I.; Naidu, B.V.K.; Aminabhavi, T.M. *J. Chem. Eng. Data* **2004**, 49, 468.

54) Xu, R; Winnik, M.A.; Riess, G.; Chu, B.; Croucher, M.D. *Macromolecules* **1992**, 25, 644.

55) Shen, H.; Eisenberg, A. *J. Phys. Chem. B* **1999**, 103, 9473.

56) Förster, S.; Zisenis, M.; Wenz, E.; Antonietti, M. *J. Chem. Phys.* **1996**, 104, 9956.

57) Zhulina, E.B.; Birshtein, T.M. *Vysokomol. Soedin.* **1985**, 27, 511.

## 9. List of abbreviations and used symbols

| | |
|---|---|
| $A$ | amplitude |
| A | core forming block |
| $A(\lambda_E)$ | absorbance |
| $A_2$ | second virial coefficient |
| AFM | atomic force microscopy |
| $\alpha_i$ | preexponential factors (amplitudes) |
| $A_{np}(\nu)$ | absorption spectrum in a nonpolar solvent |
| $A_p(\nu)$ | frequency absorption spectrum in a polar solvent |
| $B$ | correction factor to the background |
| $\beta$ | coherence factor |
| B | shell forming block |
| $C$ | coefficient depending on the slowest internal motion and polydispersity of the scattering particles |
| $c$ | molar concentration |
| $C(t)$ | correlation function |
| $\chi^2$ | goodness of fit |
| $\chi_{A-B}$ | Flory-Huggins interaction parameter between components A and B |
| CL | ε–caprolactone |
| CT | charge transfer |
| D | debye |
| $d$ | diameter |
| $\Delta$ | width parameter |
| $\delta$ | spectral shift |
| $D(\lambda,t)$ | decomposed fluorescence decay |
| $\delta_0$ | average spectral shift |
| $D_{app}$ | apparent diffusion coefficient |
| d$n$/d$c$ | refractive index increment |
| $\langle D \rangle_z$ | z-averaged diffusion coefficient with real physical meaning |
| $\Delta R(\theta,w)$ | excess Rayleigh ratio |
| $\Delta\omega$ | overall Stokes shift |

| | |
|---|---|
| $\varepsilon(\lambda_E)$ | molar absorption coefficient |
| $\boldsymbol{E}(t)$ | electric field |
| EO | ethylene oxide |
| $F(\lambda,t)$ | time-resolved emission spectrum |
| $F_{fit}(\omega,t)$ | fit of a time-resolved emission spectrum |
| $F_p(v,v_{ex},t=0)$ | time-resolved fluorescence spectrum at the time zero |
| FWHM | full width at half maximum |
| $\Gamma$ | relaxation rate |
| $\gamma$ | asymmetry parameter |
| $g_1(t)$ | normalized autocorrelation function of the electric field |
| $g_2(t)$ | normalized intensity autocorrelation function |
| $h$ | peak height |
| $\eta$ | viscosity |
| $I(\theta,w)$ | intensity of the light scattered from the unit volume to the direction given by the angle between the incident and scattered light beams |
| $I(t)$ | intensity of the scattered light at time $t$ |
| $I_0$ | intensity of the incident light |
| $I_A(\lambda_E)$ | intensity of absorbed light |
| $I_{EM}(\lambda_E,\lambda_F)$ | recorded steady state fluorescence intensity |
| $I_F(t)$ | theoretical fluorescence intensity at time $t$ after excitation |
| $I_F(t)'$ | fluorescence decay as a sum of exponentials |
| $K$ | constant |
| $k$ | arbitrary integer number |
| $\kappa$ | theoretical exponent |
| $k_B$ | Boltzmann constant |
| $k_D$ | hydrodynamic virial coefficient |
| $k_{nr}$ | constant for nonradiative deactivation |
| $k_p$ | proportionality factor |
| $k_r$ | constant for radiative deactivation |
| $\lambda$ | wavelength |
| $l$ | optical path |
| $L(t')$ | the intensity of the excitation pulse at the time $t'$ |
| LAURDAN | 6-lauroyl-2-(dimethylamino)naphthalene |

| | |
|---|---|
| LE | locally excited |
| $\lambda_E$ | excitation wavelength |
| $\lambda_F$ | emission wavelength |
| Lipase PS | Lipase Pseudomonas |
| LS | light scattering |
| $\mu$ | theoretical exponent |
| $\mu_2$ | cumulant of the second order |
| $M_w$ | weight averaged molar mass |
| $M_w^{app}$ | apparent weight average molar mass |
| $n_0$ | refractive index of a solvent |
| $\nu$ | frequency |
| $N^*$ | number of molecules which are still in the excited state |
| $N_A$ | Avoggadro's number |
| $N_{CL}$ | number of CL monomer units in the PCL-PEO polymer |
| $N_{EO}$ | number of EO monomer units in the PCL-PEO polymer |
| $\nu_{ex}$ | excitation frequency |
| $\nu_{np}$ | peak position in the frequency domain in a nonpolar medium |
| $\nu_p$ | peak position in the frequency domain in a polar medium |
| $p(\delta)$ | distribution of spectral shifts |
| $P(\theta)$ | particle scattering function |
| PATMAN | 6-hexadecanoyl-2-(((2-(trimethylamonium)ethyl)methyl)amino) naphtalene chloride |
| PBLA | poly(β-benzyl L-aspartate) |
| PBLG | poly(γ-benzyl-L-glutamate) |
| PCL($n$)-PEO | poly(ε–caprolactone)-*block*-poly(ethylene oxide) with the molar mass of PCL equal to 1000$n$ g/mol |
| $PCL_m$-$PEO_n$ | poly(ε–caprolactone)-*block*-poly(ethylene oxide) with $m$ PCL and $n$ EO monomer units |
| PDLLA | poly(D,L-lactide) |
| PPO | poly(propylene oxide) |
| PRODAN | 6-propionyl-2-(dimethylamino)naphthalene |
| PS-PVP-PEO | polystyrene-*block*-poly(2-vinylpyridine)-*block*-poly(oxyethylene) |

| | |
|---|---|
| $\theta$ | angle between the incident light and the direction of observation |
| $q$ | size of the scattering vector |
| QELS | quasi-elastic light scattering |
| $r$ | distance between the scattering volume and the detector |
| $R(t)$ | observed fluorescence decay |
| $R(t_i)$ | fitted function |
| $R_c(t_i)$ | fit of the function $R(t_i)$ |
| $\rho_{eff}$ | effective density |
| $R_g$ | z-averaged radius of gyration |
| $R_H$ | hydrodynamic radius |
| $\sigma$ | variance of a distribution |
| $S(\lambda_F)$ | steady-state emission spectrum |
| $\sigma_i$ | standard deviation |
| SLS | static light scattering |
| $S_n$ | $n$-th singlet state |
| $S_{np}(\nu)$ | steady-state emission spectrum in a nonpolar medium |
| SR | solvent relaxation |
| SSFS | steady-state fluorescence spectrum |
| SSL | strong segregation limit |
| SSSL | super strong segregation limit |
| $t$ | time |
| $T$ | temperature, timespan |
| $\tau$ | relaxation time |
| $T_1$ | first triplet state |
| $\tau A(\tau)$ | distribution of relaxation times |
| TCSPC | time-correlated single photon counting |
| THF | tetrahydrofuran |
| $\tau_i$ | lifetimes of the excited states |
| $\tau_R$ | mean correlation time |
| TRANES | time-resolved area-normalized emission spectrum |
| TRES | time-resolved emission spectrum |
| $\upsilon$ | number of degrees of freedom |
| $w$ | mass concentration |

| | |
|---|---|
| $\omega$ | wavenumber |
| $\omega$(peak,$t$) | peak position in the wavenumber domain |
| $w_f$ | mass concentration of the polymer in the final solvent |
| $w_i$ | mass concentration of the polymer in the initial solvent |
| WSL | weak segregation limit |
| $Z$ | particle-aggregation number |

## 10. Publications

Šachl, R.; Uchman M.; Matějíček, P.; Procházka, K.; Štěpánek, M.: Preparation and Characterization of Self-assembled Nanoparticles Formed by Poly(ethylene oxide)-*block*-poly($\varepsilon$-caprolactone) Copolymers with Long Poly($\varepsilon$-caprolactone) Blocks in Aqueous Solutions *Langmuir* **2007**, 23, 3395.

# Preparation and Characterization of Self-Assembled Nanoparticles Formed by Poly(ethylene oxide)-*block*-poly(ϵ-caprolactone) Copolymers with Long Poly(ϵ-caprolactone) Blocks in Aqueous Solutions

Radek Šachl, Mariusz Uchman, Pavel Matějíček, Karel Procházka, and Miroslav Štěpánek*

*Department of Physical and Macromolecular Chemistry, Faculty of Science, Charles University in Prague, Albertov 2030, 128 40 Prague 2, Czech Republic*

Milena Špírková

*Institute of Macromolecular Chemistry, Academy of Sciences of the Czech Republic, Heyrovský Square 2, 162 06 Prague 6, Czech Republic*

*Received October 13, 2006. In Final Form: December 15, 2006*

Aqueous solutions of self-assembled nanoparticles formed by biocompatible diblock copolymers of poly(ϵ-caprolactone)-*block*-poly(ethylene oxide) (PCL-PEO) with the same molar mass of the PEO block (5000 g mol$^{-1}$) and three different molar masses of the PCL block (5000, 13 000, and 32 000 g mol$^{-1}$) have been prepared by a fast mixing the copolymer solution in a mild selective solvent, tetrahydrofuran (THF)/water, with an excess of water, that is, by quenching the reversible micellization equilibrium, and a subsequent removal of THF by dialysis of the water-rich solution against water. The prepared nanoparticles have been characterized by static and dynamic light scattering and atomic force microscopy imaging. It was found that stable monodisperse nanoparticles are formed only if the initial mixed solvent contained 90 vol % THF. The results show that the prepared nanoparticles are spherical vesicles with relatively thick hydrophobic walls, that is, spherical core/shell nanoparticles with the hollow core filled with the solvent.

## Introduction

The potential application of self-assembled nanoparticles formed by different amphiphilic polymers as vessels for controlled drug release and/or targeted drug delivery in pharmacology has been a subject of numerous studies.[1] Most investigations deal with nanoparticles of AB diblock and ABA- or BAB-type triblock copolymers, where A is a hydrophobic, core-forming block, and B is a hydrophilic, shell-forming block. In many systems, the hydrophilic block is poly(ethylene oxide), PEO, because particles coated by this polymer are tolerated by living organisms and exhibit very low adsorption affinity to proteins.[2] The core-forming blocks are usually polymers that undergo hydrolysis in aqueous solutions and decompose, that is, polyamides, like poly(γ-benzyl-L-glutamate)[3] and poly(β-benzyl-L-aspartate),[4] or polyesters, like poly(DL-lactide)[5] and poly(ϵ-caprolactone) (PCL).[6] Nanoparticles formed by such block copolymers in aqueous solutions are thus both biocompatible and biodegradable, and their cores are able to solubilize various hydrophobic compounds.

Nanoparticles of PCL and PEO diblock or triblock copolymers have been studied as carrier vessels for the immunosuppressive Cyclosporine,[6] the calcium antagonist Nimodipine,[7] and other drugs. Most studies of PCL-PEO and PCL-PEO-PCL micelles, as drug delivery vessels, concentrate on their preparation and characterization[8,9] and on kinetic studies of the release of solubilized compounds[6,7] to the bulk solution or their decomposition both in vitro[10,11] and in vivo.[12]

As water is an extremely strong precipitant for hydrophobic blocks of the above-mentioned copolymers, their direct dissolution in water is either difficult or impossible. Vangeyte et al.[8] prepared nanoparticles of PCL-PEO diblock copolymers with relatively short PCL blocks ($M_n$ not exceeding 3900 g mol$^{-1}$) by direct dissolution of the copolymer in water at 80 °C, but this procedure cannot be used for the preparation of nanoparticles from amphiphilic copolymers with a long hydrophobic block.

The most common method of preparation of aqueous solutions of nanoparticles formed by amphiphilic block copolymers is the dissolution of the copolymer in a mixture of a good solvent for the hydrophobic block with water, in which the reversible multimolecular micelles with swollen cores form spontaneously. The organic solvent content is subsequently decreased by the injection of the solution in an excess of water, by distillation, or by dialysis of the solution against water. The thermodynamic quality of the solvent for the hydrophobic blocks deteriorates with decreasing content of the organic solvent, and the association number increases.[13] A further decrease in the content of the organic solvent causes the collapse of hydrophobic cores, and the nanoparticles kinetically "freeze". Their association number does not change any more. Nevertheless, it depends on the

* Corresponding author. E-mail: stepanek@natur.cuni.cz.

(1) Kataoka, K.; Harada, A.; Nagasaki, Y. *Adv. Drug Delivery Rev.* **2001**, *47*, 113.
(2) Claesson, P. *Colloids Surf., A* **1993**, *77*, 109.
(3) Nah, J. W.; Jeong, Y. I.; Cho, C. S.; Kim, S. I. *J. Appl. Polym. Sci.* **2000**, *75*, 1115.
(4) Yu, B. G.; Okano, T.; Kataoka, K.; Sardari, S.; Kwon, G. S. *J. Controlled Release* **1998**, *56*, 285.
(5) Lee, J. Y.; Cho, E. C.; Cho, K. *J. Controlled Release* **2004**, *94*, 323.
(6) Aliabadi, H. M.; Brocks, D. R.; Lavasanifar, A. *Biomaterials* **2005**, *26*, 7251.
(7) Ge, H.; Hu, Y.; Jiang, X.; Cheng, D.; Yuan, Y.; Bi, H.; Yang, C. *J. Pharm. Sci.* **2002**, *91*, 1463.
(8) Vangeyte, P.; Leyh, B.; Heinich, M.; Grandjean, J.; Bourgaux, C.; Jérôme, R. *Langmuir* **2004**, *20*, 8442.
(9) Vangeyte, P.; Gautier, S.; Jérôme, R. *Colloids Surf., A* **2004**, *242*, 203.
(10) Gan, U.; Jim, T. F.; Li, M.; Yuer, Z.; Wang, S.; Wu, C. *Macromolecules* **1999**, *32*, 590.
(11) Nie, T.; Zhao, Y.; Xie, Z.; Wu, C. *Macromolecules* **2003**, *36*, 8825.
(12) Savi, R.; Azzam, T.; Eisenberg, A.; Maysinger, D. *Langmuir* **2006**, *22*, 3570.
(13) Tuzar, Z.;Webber, S. E.; Ramireddy, C.; Munk, P. *Polym. Prepr. (Am. Chem. Soc., Div. Polym. Chem.)* **1991**, *32*, 525.

10.1021/la063014c CCC: $37.00 
Published on Web 02/02/2007

copolymer concentration, its composition and architecture, rate of the organic solvent removal, temperature, and other factors. The fact that the association number and size of resulting nanoparticles can be influenced by the modification of the preparation protocol is very promising for potential applications in medicine. It allows for tuning the properties of the delivery vessel and minimizes the number of syntheses of samples differing in length and chemical composition. Vangeyte et al.[9] demonstrated that the choice of the organic solvent and the method of the copolymer transfer from the mild selective solvent into the aqueous solution affect the self-assembly of the PCL-PEO block copolymer.

The small-angle X-ray and neutron scattering measurements revealed that PCL-PEO nanoparticles prepared by direct dissolution of the copolymer in water at elevated temperature are spherical micelles of about 20 nm in diameter.[8] However, the nanoparticles prepared using an organic cosolvent were found substantially larger. Their hydrodynamic radius measured by dynamic light scattering ranges up to 50 nm, and with respect to the lengths of both core- and shell-forming blocks the formed particles are too large to possess the micellar structure.[9]

In this paper, we report on the preparation and characterization of nanoparticles formed by PCL-PEO copolymers in aqueous solutions. Unlike in refs 8 and 9, we use the PCL-PEO copolymers whose PCL blocks have the same length or are longer than the PEO block, which results in very poor solubility in water. The used preparation protocol is based on the injection of PCL-PEO dissolved in tetrahydrofurane (THF)-rich aqueous mixtures into an excess of water. For the characterization of prepared nanoparticles, we employ static and dynamic light scattering and atomic force microscopy.

## Experimental Section

**Materials.** *Copolymer Samples.* Three PCL-PEO samples, PCL(5)-PEO, PCL(13)-PEO, and PCL(32)-PEO, all with the declared polydispersity index less than 1.4, were purchased from Aldrich. The numbers in brackets indicate number-averaged molar masses, $M_n$, of the PCL block in kg/mol; $M_n$ of the PEO blocks was 5 kg/mol for all three samples.

*Preparation of Nanoparticles.* The aqueous solutions of PCL-PEO nanoparticles were prepared according to the following protocol: 10 mg of each copolymer was added to 2 mL of THF or THF/water mixtures differing in composition and left shaken overnight. Full dissolution of all three copolymers was achieved in THF/water mixtures containing more than 60 vol % of THF. The THF-rich solutions were then added drop-by-drop to 4 mL of water under vigorous stirring. Finally, the solutions were dialyzed extensively against water several times to remove THF completely.

*Solvents.* THF, luminescence spectroscopy grade, from Fluka, and deionized water were used as solvents.

**Techniques.** *Light Scattering Measurements.* The light scattering setup (ALV, Langen, Germany) consisted of a 633 nm He−Ne laser, an ALV CGS/8F goniometer, an ALV High QE APD detector, and an ALV 5000/EPP multibit, multitau autocorrelator. The solutions for measurements were filtered through 0.45 $\mu$m Acrodisc filters. The measurements were carried out for different concentrations (0.4−1.8 g/L) and different angles at 20 °C.

Static light scattering (SLS) measurements were treated by the Berry method using the equation:

$$\sqrt{\frac{Kc}{R(q,c)}} = \sqrt{\frac{1}{M_w}}\left(1 + \frac{1}{6}R_g^2 q^2\right)(1 + A_2 M_w c) \qquad (1)$$

where $M_w$, $R_g$, and $A_2$, respectively, are the weight-averaged molar mass, $z$-averaged radius of gyration, and the "light-scattering-averaged" osmotic second virial coefficient of the polymer in the solution, and $R(q,c)$ is the corrected Rayleigh ratio that depends on the polymer concentration $c$ and on the magnitude of the scattering vector $q = (4\pi n_0/\lambda)\sin(\vartheta/2)$, where $\vartheta$ is the scattering angle, $n_0$ is the refractive index of the solvent, and $\lambda$ is the wavelength of the incident light. The contrast factor $K$ is given by the relationship $K = 4\pi^2 n_0^2 (dn/dc)^2/(\lambda^4 N_A)$, where $(dn/dc)$ is the refractive index increment of the polymer with respect to the solvent, and $N_A$ is the Avogadro constant.

Refractive index increments of PCL-PEO samples were calculated as the weighted average of literature data for PCL and PEO on the basis of copolymer compositions.[14,15] As PCL is water-insoluble and the pertinent value in water is thus not available, the literature $dn/dc$ value for PCL in THF[15] was recalculated to that in water, assuming that, in the first approximation, the difference between increments in two solvents equals the difference of refractive indices of the solvents.[16] The same approximation was employed for the calculation of increments in mixed THF/water solvents, using the literature data on the refractive index dependence on the composition of THF/water mixtures.[17] We compared the values of $(dn/dc)$ for 90% THF, in which the copolymers are directly soluble, obtained by the measurement with a Brice−Phoenix differential refractometer with those calculated by this procedure, and the results agreed very well for all three samples. Therefore, the used approximation should neither invalidate nor significantly affect the data.

Dynamic light scattering measurements were evaluated by fitting of the measured normalized time autocorrelation function of the scattered light intensity, $g_{(2)}(t)$, related to the electric field autocorrelation function, $g_{(1)}(t)$, by the Siegert relation, $g_{(2)}(t) = 1 + \beta|g_{(1)}(t)|^2$. The data were fitted with the aid of the constrained regularization algorithm (CONTIN), which provides the distribution of relaxation times $\tau$, $A(\tau)$, as the inverse Laplace transform of $g_{(1)}(t)$ function:

$$g_{(1)}(t) = \int_0^\infty A(\tau)\exp(-t/\tau)\,d\tau \qquad (2)$$

To obtain the averaged hydrodynamic radius of the particles, $R_H$ ($z$-average for $R_H^{-1}$), the $g_{(1)}(t)$ functions for various copolymer concentrations and scattering angles were fitted to the second-order cumulant expansion:

$$g_{(1)}(t) = \exp(-D_{app}q^2 t + \mu_2 t^2/2) \qquad (3)$$

where $D_{app}$ is the apparent diffusion coefficient, and $\mu_2$ (the second cumulant) is the second moment of the distribution function of relaxation times. The $D_{app}$ values obtained from the fits were further extrapolated to zero $q$ and $c$ to yield the $z$-averaged diffusion coefficient of the particles, $\langle D\rangle_z$, using the relationship:[18]

$$D_{app}(q,c) = \langle D\rangle_z(1 + k_D c + C R_g^2 q^2) \qquad (4)$$

where $k_D$ is the hydrodynamic virial coefficient, and $C$ is a coefficient determined by the slowest internal motion and polydispersity of the scattering particles. The hydrodynamic radius was calculated from $\langle D\rangle_z$, by means of the Stokes−Einstein formula:

$$R_H = \frac{k_B T}{6\pi\eta_0\langle D\rangle_z} \qquad (5)$$

where $k_B$ is the Boltzmann constant, $T$ is the temperature, and $\eta_0$ is the viscosity of the solvent.

*Atomic Force Microscopy (AFM).* Atomic force microscopy measurements were performed in the tapping mode under ambient conditions using a commercial scanning probe microscope, Digital

(14) *Polymer Handbook*, 3rd ed.; Brandup, J., Immergut, E. H., Eds.; Wiley Interscience: New York, 1989.
(15) Wu, C.; Woo, K. F.; Luo, X.; Ma, D.-Z. *Macromolecules* **1994**, *27*, 6055.
(16) Huglin, M. B. In *Light Scattering from Polymer Solutions*; Huglin, M.B., Ed.; Academic Press: London, 1972; pp 165−331.
(17) Nayak, J. N.; Aralaguppi, M. I.; Naidu, B. V. K.; Aminabhavi, T. M. *J. Chem. Eng. Data* **2004**, *49*, 468.
(18) Burchard, W. In *Light Scattering. Principles and Development*; Brown, W., Ed.; Clarendon Press: Oxford, 1996; pp 439−476.

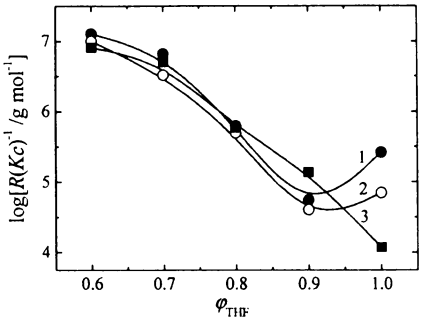


**Figure 1.** Logarithm of the apparent molar mass ($R/Kc$ at the scattering angle $\vartheta = 90°$) of PCL(5)-PEO (curve 1), PCL(13)-PEO (curve 2), and PCL(32)-PEO (curve 3) aggregates in THF/water mixtures, as a function of THF volume fraction, $\varphi_{THF}$. The mass concentration of the copolymers in the solutions was $c = 1$ g L$^{-1}$.

Instruments NanoScope dimensions 3, equipped with a Nanosensors silicon cantilever, typical spring constant 40 N m$^{-1}$. Nanoparticles were deposited on a fresh (i.e., freshly peeled out) mica surface (flogopite, theoretical formula $KMg_3AlSi_3O_{10}(OH)_2$, Geological Collection of Charles University in Prague, Czech Republic) by a fast dip coating in a dilute PCL-PEO solution in water ($c$ of ca. $10^{-2}$ g L$^{-1}$). After the evaporation of water, the samples for AFM were dried in a vacuum oven at ambient temperature for ca. 5 h.

## Results and Discussion

**Characterization of PCL-PEO Nanoparticles by Light Scattering.** To find the optimum composition of the mixed solvent for the preparation of well-defined PCL-PEO nanoparticles in aqueous media, we varied the composition of THF/water mixtures, from which the dissolved copolymers were transferred into aqueous solutions, and characterized the copolymer associates formed in these solvents.

Not surprisingly, the solubility of the PCL-PEO copolymers in THF/water mixtures decreases with increasing length of the water-insoluble PCL block. The minimum THF content in THF/water mixtures for the complete dissolution of all three samples (1 mL of the solvent per 5 mg of the copolymer) was 60 vol %.

Figure 1 shows the dependence of the scattering intensity at the scattering angle $\vartheta = 90°$, of the PCL-PEO solutions in THF/water mixtures on the volume fraction of THF. The changes are large, and the scattering intensity was expressed as $R/Kc$ (i.e., the apparent molar mass). The refractive index increments of the copolymers for individual mixed solvents were determined as described in the Experimental Section. The measured quantity, which is roughly proportional to the molar mass of the PCL-PEO aggregates formed in THF/water solutions, decreases with increasing volume fraction of THF, $\varphi_{THF}$, until $\varphi_{THF} = 0.9$ where it passes a minimum for PCL(5)-PEO and PCL(13)-PEO. In pure THF, which is a poor solvent for PEO, the copolymers aggregate due to limited solubility of PEO blocks, and $R/Kc$ thus increases with the increasing weight fraction of PEO in the copolymer.

The injection of PCL-PEO solutions in THF-rich/water mixtures in an excess of water leads to the formation of stable nanoparticles only in the case of the copolymer solutions in 80% and 90% THF. The DLS relaxation time distributions of final aqueous solutions (i.e., after removal of THF by dialysis) are plotted in Figure 2, which shows that the best results (unimodal, relatively narrow distributions for all three samples) were achieved if the initial solvent contained 90% THF, in which the PCL-(5)-PEO and PCL(13)-PEO copolymers formed aggregates with the lowest apparent molar mass. With 80% THF as the initial solvent, the relaxation time distributions for final aqueous

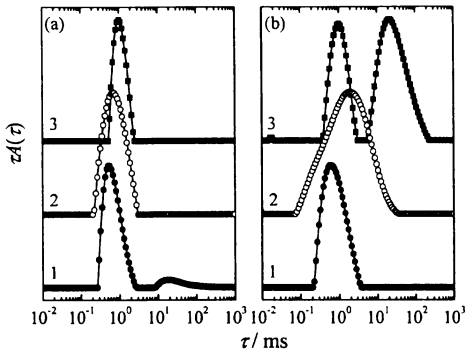


**Figure 2.** DLS relaxation time distributions (measured at the scattering angle $\vartheta = 90°$) of PCL(5)-PEO (curve 1), PCL(13)-PEO (curve 2), and PCL(32)-PEO (curve 3) aqueous solutions prepared from copolymer solutions in (a) 90% THF and (b) 80% THF (the final copolymer concentration, $c = 0.4$ g L$^{-1}$).

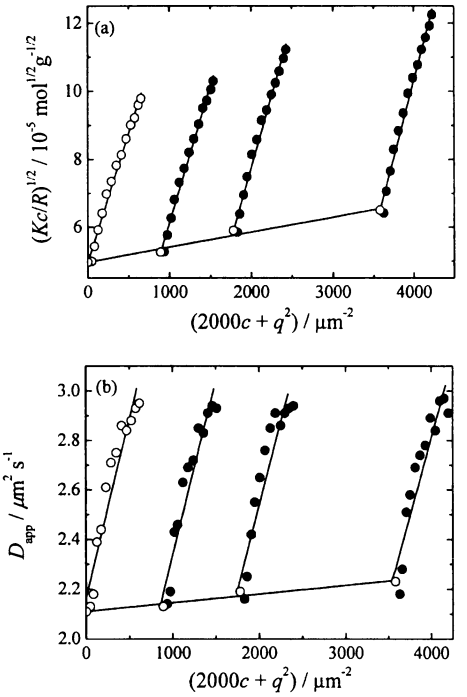


**Figure 3.** (a) The Berry plot and (b) the dynamic Zimm plot of light scattering data for PCL(32)-PEO aqueous solutions.

solutions are broader and in the case of PCL(32)-PEO nanoparticles even bimodal (curve 3 in Figure 2b). The admixture of the large aggregates in the PCL(32)-PEO aqueous solution can be explained as a consequence of the copolymer polydispersity: The system is close to the solubility limit, and the small fraction PCL(32)-PEO chains with longer PCL blocks (i.e., less soluble chains in aqueous solutions) tend to precipitate and form large aggregates. (One has to keep in mind that the shown distibutions are intensity-weighted and the aggregates scatter much stronger than the small nanoparticles. The mass fraction of the aggregates is thus very small.)

For other THF/water solvent compositions, highly turbid unstable suspensions of PCL-PEO nanoparticles precipitating on the time scale of days were formed after their transfer into aqueous media. Therefore, only the aqueous solutions prepared from the PCL-PEO solutions in 90 vol % THF were used for further study.

**Table 1. Molecular Characteristics of PCL-PEO Nanoparticles in Aqueous Solutions**

| copolymer | $M_w \times 10^{-6}$, g mol$^{-1}$ | $R_g$, nm | $R_H$, nm | $R_g/R_H$ | $Z$ | $\rho$, g cm$^{-3}$ |
|---|---|---|---|---|---|---|
| PCL(5)-PEO | 22.7 ± 0.2 | 40 ± 1 | 42.2 ± 0.7 | 0.95 ± 0.04 | 2270 ± 5 | 0.12 ± 0.01 |
| PCL(13)-PEO | 77.6 ± 1.5 | 57 ± 1 | 60.7 ± 0.3 | 0.94 ± 0.02 | 4310 ± 60 | 0.13 ± 0.01 |
| PCL(32)-PEO | 406 ± 16 | 96 ± 2 | 99 ± 3 | 0.97 ± 0.05 | 10 900 ± 1800 | 0.16 ± 0.02 |

Figure 3a and b shows the Berry plot (SLS data) and the dynamic Zimm plot (i.e., $D_{app}$ vs $kc + q^2$ from DLS data), respectively, for PCL(32)-PEO nanoparticles in water transferred from the solution in 90 vol % THF. The results of measurements for PCL(5)-PEO and PCL(13)-PEO solutions are qualitatively similar and are not shown. The concentration dependences of the scattered intensity and distributions of relaxation times do not indicate any dissociation of nanoparticles at low concentrations and confirm the assumption that the nanoparticles are kinetically frozen.

The molecular characteristics of PCL-PEO nanoparticles obtained by light scattering for the aqueous solutions obtained by quenching the solutions in 90 vol % THF are summarized in Table 1, together with other parameters, that is, $R_g/R_H$ ratio, aggregation number, $Z$, calculated as $Z = M_w/(M_n)_u$, where $(M_n)_u$ is the number-averaged molar mass of the unimers, and the average density, $\rho$, is given by the relationship $\rho = 3M_w/(4\pi N_A R_H^3)$.

It is interesting and slightly surprising that the association number of micelles follows the scaling relation fairly well despite the fact that the prepared PCL-PEO micelles are kinetically frozen nonequilibrium nanoparticles. In this case, their molar mass should depend mainly on the preparation protocol. According to our opinion, it is due to the fact that the used protocol is based on quenching, that is, on a fast transfer from the fully reversible equilibrium state (for all three samples) to conditions that are very bad for the PCL core. In Figure 4, log $Z$ is plotted as a function of the logarithm of the number of PCL units. The fit of the data yields the relation $Z \approx N_{PCL}^{\mu}$, where $\mu = 0.85$ is the scaling exponent.

Although this value fits between exponents predicted by the scaling theory[19] (i) for the model of the hairy micelle with the core negligibly small in comparison with the size of the shell, $\mu = {}^4/_5$, and (ii) for the model of the crew cut micelle whose size is approximately the same as the size of its core, $\mu = 1$, one must bear in mind that PCL-PEO micelles in aqueous solutions should exhibit different scaling relations. Micelles of amphiphilic copolymers such as PCL-PEO in aqueous solutions are characterized by large Flory–Huggins interaction parameters $\chi_{AB}$ and $\chi_{AS}$, where indices A, B, and S refer to the core-forming block monomer, the shell-forming block monomer, and the solvent, respectively. These values correspond to a strong segregation of (i) the core from the shell and (ii) the solvent from the core. For micelles under such conditions, the scaling theory[19] predicts $Z \approx N_A^2$, irrespective of the ratio between $N_A$ and $N_B$. The validity of this scaling relation was confirmed experimentally for polystyrene-*block*-poly(4-vinylpyridine) micelles in toluene[20] and for polystyrene-*block*-poly(methacrylic acid) micelles in dioxane(80 vol %)/water mixture,[21] where the experimental scaling exponents $\mu$ were found to be 1.93 and 1.89, respectively.

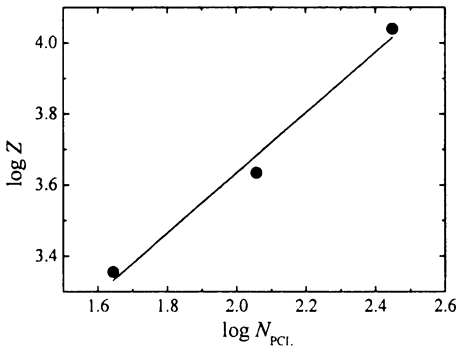


**Figure 4.** Logarithm of the aggregation number, $Z$, of PCL-PEO nanoparticles as a function of the logarithm of the number of PCL units, $N_{PCL}$.

Not only the observed scaling relation but also the sizes and molar masses of PCL-PEO nanoparticles are slightly surprising. The nanoparticles are clearly too large and their aggregation numbers are too high for simple core/shell micelles. For comparison, Winnik et al. found that diblock copolymers of polystyrene-*block*-poly(ethylene oxide) with molar masses from 8.5 to 50.8 kg/mol formed the core/shell micelles with hydrodynamic radii ranging from 10 to 23 nm and aggregation numbers from 350 to 1850.[22] However, hydrodynamic radii of about 50 nm and aggregation numbers of about 5000, that is, values comparable to those obtained in this study, were reported by Eisenberg et al. for vesicles formed by asymmetrical polystyrene-*block*-poly(acrylic acid) with molar masses 32 and 4 kg/mol for polystyrene and poly(acrylic acid) blocks, respectively.[23] This comparison suggests that the prepared PCL-PEO nanoparticles could have the vesicle-like structure.

Block copolymer vesicles, also called polymersomes,[23–26] have a concentric spherical structure similar to that of liposomes (phospholipid vesicles); that is, they contain a cavity filled with the solvent, surrounded by a spherical layer formed by insoluble blocks, which is separated from the solvent inside by an inner layer and from outside by an outer layer, both formed by soluble blocks of the same type. Besides the high association numbers, two following observations support the assumption of the vesicular structure of PCL-PEO nanoparticles:

(i) The measured $R_g/R_H$ ratios are close to the theoretical value for the hollow sphere, $(R_g/R_H)_{hs} = 1$. The slightly lower values obtained by light scattering could be caused by the polydispersity and finite wall thickness of the formed vesicles.

(ii) The average densities of the nanoparticles are relatively low, indicating that a major part of the nanoparticle volume should be filled with the solvent. As the solvent-swollen shells of the nanoparticles are formed by relatively short PEO chains, such low-density values suggest the presence of the solvent also in a cavity in the nanoparticle core.

There is also a supporting argument for the formation of vesicles in our system raising from the observations of Luo and Eisenberg,[24] who showed that block copolymer vesicles are

(19) Zhulina, E. B.; Birshtein, T. M. *Vysokomol. Soedin.* **1985**, *27*, 511.
(20) Förster, S.; Zisenis, M.; Wenz, E.; Antonietti, M. *J. Chem. Phys.* **1996**, *104*, 9956.
(21) Qin, A.; Tian, M.; Ramireddy, C.; Webber, S. E.; Munk, P.; Tuzar, Z. *Macromolecules* **1994**, *27*, 120.
(22) Xu, R.; Winnik, M. A.; Riess, G.; Chu, B.; Croucher, M. D. *Macromolecules* **1992**, *25*, 644.
(23) Shen, H.; Eisenberg, A. *J. Phys. Chem. B* **1999**, *103*, 9473.
(24) Luo, L.; Eisenberg, A. *J. Am. Chem. Soc.* **2001**, *123*, 1012.
(25) Bermudez, H.; Brannan, A. K.; Hammer, D. A.; Bates, F. S.; Discher, D. E. *Macromolecules* **2002**, *35*, 8203.
(26) Ortiz, V.; Nielsen, S. O.; Discher, D. E.; Klein, M. L.; Lipowsky, R.; Shillcock, J. *J. Phys. Chem. B* **2005**, *109*, 17708.

stabilized by segregation of chains with short hydrophilic blocks to the inside of the vesicles and of the long hydrophilic chains to the outside. This mechanism of vesicle stabilization is especially relevant in our case with respect to the relatively high polydispersity ($M_w/M_n$ is ca. 1.4) of the PCL-PEO copolymers.

However, the copolymer vesicles prepared and described, for example, by Eisenberg et al.[23] exhibit broad size distributions, while the wall thickness distributions are relatively narrow. On the contrary, the radii of the studied PCL-PEO nanoparticles are controlled by copolymer molar masses, which suggests that their cavities are fairly small.

Because all structural characteristics obtained by light scattering are indirect, the question of the shape and inner structure of nanoparticles cannot by solved by LS only. Hence, we performed an additional study of PCL-PEO nanoparticles by atomic force microscopy, as described in the following section.

**Atomic Force Microscopy Imaging of PCL-PEO Nanoparticles.** For the atomic force microscopy study, the PCL-PEO nanoparticles were deposited from aqueous solutions on a freshly peeled-off mica surface. When comparing AFM data with results of techniques used for studying the solutions, one has to be careful. The thermodynamic conditions and forces acting on polymeric nanoparticles at the surface are very different from those in the solution before deposition. Hence, the nanoparticles may reorganize, for example, aggregate or decompose, during the deposition on the mica surface. On the basis of the experience gained in our earlier studies,[27-29] we do believe that we can (i) decide if the comparison is relevant or not (i.e., if an important reorganization occurred or not), in the case that the AFM study is relevant, (ii) prevent or, at least, substantially minimize the effect of complicating factors (by tuning the conditions during the deposition), and finally (iii) differentiate between the core/shell micelles and vesicles.

Figure 5a and b, respectively, shows the top view of 1 $\mu$m × 1 $\mu$m scans of PCL(5)-PEO and PCL(32)-PEO nanoparticles. (Scans of PCL(13)-PEO nanoparticles are similar to those of PCL(32)-PEO and are not shown.) The images show clearly that many particles are "ring-shaped", with a hollow space in the center. The horizontal profiles of the "ring-shaped" particles obtained by the section analysis of both scans are shown in Figure 6.

In our earlier study,[27] we found that, if major complications are prevented, sizes of block copolymer micelles evaluated from AFM scans are proportional to those measured in the solution by light scattering, although the deposited micelles are pancake-deformed due to their interaction with the surface and their heights correspond approximately to the core diameter. The pancake deformation is observed also in the case of PCL-PEO nanoparticles. The section analysis of the sizes and shapes of PCL(5)-PEO and PCL(32)-PEO nanoparticles provides roughly the same horizontal diameter for both particles, $D$, about 220 nm, as well as the same diameter of the hollow center. The diameter, estimated in the half of the particle height, is ca. 40 nm. The particles formed by different samples differ significantly in the height, which is ca. 6 nm for PCL(5)-PEO and 12 nm for PCL(32)-PEO. The presence of the hollow space in the center of the deposited nanoparticles supports the assumption that the nanoparticles are vesicles, because the presence of a "crater" can be explained as a result of the collapse of the vesicle wall after the evaporation of the solvent.

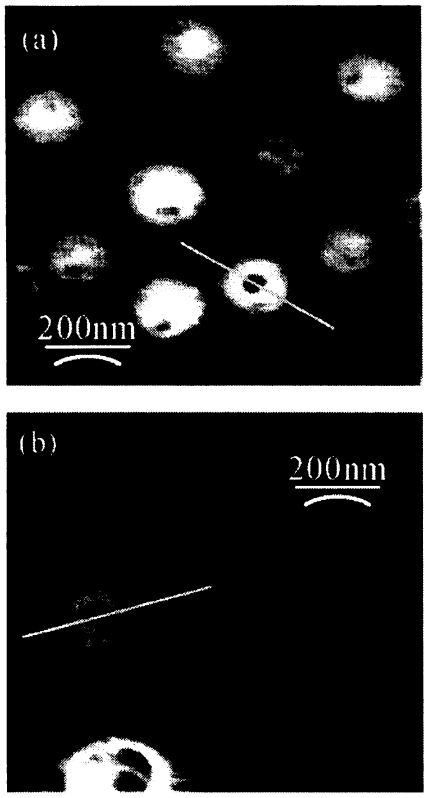


**Figure 5.** AFM scans (top view, 1 $\mu$m × 1 $\mu$m) of (a) PCL(5)-PEO and (b) PCL(32)-PEO nanoparticles deposited on the mica surface.

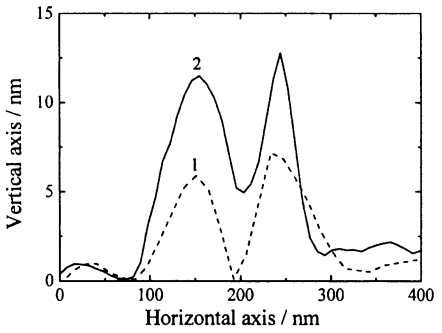


**Figure 6.** Section analysis of AFM scans of typical PCL(5)-PEO and PCL(32)-PEO nanoparticles deposited on the mica surface, curves 1 and 2, respectively.

## Conclusions

In this paper, we report on the preparation of aqueous solutions of nanoparticles formed by poly($\epsilon$-caprolactone)-*block*-poly(ethylene oxide) copolymer and their characterization by static and dynamic light scattering and atomic force microscopy. We studied three copolymer samples, with the same length of the PEO block (5 kg mol$^{-1}$) and with different lengths of the PCL blocks (5, 13, and 32 kg mol$^{-1}$). We employed tetrahydrofuran/water mixtures as initial mild selective solvents, from which the reversible and spontaneously formed nanoparticles were transferred (quenched) by fast injection into an excess of water. The preparation of purely aqueous solutions was accomplished by extensive dialysis of water-rich solutions against water for the complete removal of THF. The results of the study are as follows:

(27) Matějíček, P.; Humpolíčková, J.; Procházka, K.; Tuzar, Z.; Špírková, M.; Hof, M.; Webber, S. E. *J. Phys. Chem. B* **2003**, *107*, 8232.
(28) Humpolíčková, J.; Procházka, K.; Hof, M.; Tuzar, Z.; Špírková, M. *Langmuir* **2003**, *19*, 4111.
(29) Štěpánek, M.; Matějíček, P.; Humpolíčková, J.; Procházka, K. *Langmuir* **2005**, *21*, 10783.

(i) The best results in terms of stability and polydispersity of the prepared nanoparticles were achieved when the initial THF/water mixture contained 90 vol % of THF.

(ii) The aggregation numbers, $Z$, and hydrodynamic radii, $R_H$, of the nanoparticles in aqueous solution prepared by quenching from solutions in 90% THF are 2270 and 42 nm, 4310 and 61 nm, and 10 900 and 99 nm for PCL(5)-PEO, PCL(13)-PEO, and PCL(32)-PEO, respectively. The values of $Z$ scale with the number of PCL units, $N_{PCL}$, as $Z \approx N_{PCL}^{0.85}$. High values of both $Z$ and $R_H$ with respect to the molar mass of the copolymers suggest that the nanoparticles are rather vesicles than micelles.

(iii) AFM scans of PCL-PEO nanoparticles deposited on the mica surface show that the deposited nanoparticles are "ring-shaped". The presence of hollow centers of nanoparticles deposited on mica supports the assumption that the nanoparticles are vesicles (polymersomes) with the cavity inside the PCL core, filled with PEO blocks and the solvent.

**Acknowledgment.** K.P. acknowledges financial support from the Grant Agency of the Czech Republic (Grant No. 203/04/0490) and from the Marie Curie Research and Training Network (Grant No. 505 027, POLYAMPHI). We thank Dr. Petr Kadlec from the Institute of Macromolecular Chemistry for the measurement of refractive index increments.

LA063014C